Chapter 8
Characterizing Outbreak Trajectories and the Effective Reproduction Number

8.1 Introduction

Emerging and re-emerging infectious diseases pose major challenges to public health worldwide (Fauci and Morens 2016). Fortunately mathematical and statistical inference and simulation approaches are part of the toolkit for guiding prevention and response plans. As the recent 2013–2016 Ebola epidemic exemplified, an unfolding infectious disease outbreak often forces public health officials to put in place control policies in the context of limited data about the outbreak and in a changing environment where multiple factors positively or negatively impact local disease transmission (Chowell et al. 2017). Hence, the development of public health policies could benefit from mathematically rigorous and computationally efficient approaches that comprehensively assimilate data and model uncertainty in real time in order to (1) estimate transmission rates, (2) assess the impact of control interventions (vaccination campaigns, behavior changes), (3) test hypotheses relating to transmission mechanisms, (4) evaluate how behavior changes affect transmission dynamics, (5) optimize the impact of control strategies, and (6) generate forecasts to guide interventions in the short and long terms.

Mathematical models are quantitative frameworks with which scientists can assess hypotheses on the potential underlying mechanisms that explain patterns in the observed data at different spatial and temporal scales (Chowell 2017). Model

Electronic Supplementary Material The online version of this chapter (https://doi.org/10.1007/978-3-030-21923-9_8) contains supplementary material, which is available to authorized users.

P. Yan, G. Chowell, *Quantitative Methods for Investigating Infectious Disease Outbreaks*, Texts in Applied Mathematics 70,
https://doi.org/10.1007/978-3-030-21923-9_8

complexity can be characterized in terms of the number of variables and parameters that characterize the dynamic states of the system, spatial-temporal resolution (e.g., discrete vs. continuous time), and design (e.g., deterministic or stochastic). While agent-based models, formulated in terms of characteristics and interactions among individual agents, have become increasingly used to model detailed processes often occurring at multiple scales (e.g., within host vs. population level), mean-field models based on systems of ordinary differential equations are widely used in the biological and social sciences. These dynamic models comprise systems of equations and their parameters that together quantify the temporal and spatial states of the system via a set of interrelated dynamic quantities (e.g., susceptibility levels, disease prevalence) (Banks et al. 2009, 2014).

In Sect. 7.1, phenomenological population models refer to stochastic and deterministic models based on conceptual assumptions regarding the population. We used the term phenomenological to distinguish models with respect to assumptions at the level of individuals along the progression of the disease's natural history. We stated that phenomenological population models carry tacit assumptions at the level of individuals.

Deterministic models composed by a system of ordinary differential equations follow this general form:

$$\begin{aligned} x_1^{'}(t) &= f_1(x_1, \cdots, x_h; \Theta) \\ x_2^{'}(t) &= f_2(x_1, \cdots, x_h; \Theta) \\ &\vdots \\ x_h^{'}(t) &= f_h(x_1, \cdots, x_h; \Theta) \end{aligned}$$

where $x_i^{'}(t)$ denotes the rate of change of the system states x_i, $i = 1, \ldots, h$ and $\Theta = (\theta_1, \ldots, \theta_m)$ is the set of model parameters.

In general, the complexity of a model is a function of the parameters that are needed to characterize the states of the system and the spectrum of the dynamics that can be recovered from the model (e.g., number of equilibrium points, oscillations, bifurcations, chaos). A trade-off exists between the level of model complexity and the ability to reliably constrain a model to a specific situation.

8.2 Approximations with Simple Functions

Time-series, loosely called "epi-curves," are widely used in epidemiologic investigation for different purposes. Some make empirical comparisons for spatial and temporal patterns based on data from official surveillance reports. For example, Schanzer et al. (2010) compared epidemic curves on weekly confirmed seasonal influenza-A cases in Canada for multiple influenza seasons as well as with similar

curves in the United States and Europe. Some associate the comparison of spatial patterns with important scientific questions in mind, such as making inferences on transmissibility R_0 and disease impact such as mortality (e.g., Chowell et al. 2007). Others use epidemic curves as information for action. During an infectious disease outbreak, the question of concern is more likely about the current status of the trend, whether it is increasing or decreasing. Sometimes various ad hoc curve fitting techniques are employed to smooth fluctuating data points in order to make short-term projections, forecast health care needs, guide public health decision making, and so on.

In this section, we choose phenomenological models with explicit simple forms such as the sub-exponential function (4.58), the logistic growth (4.59), and various generalized logistic growth functions. As previously discussed in Chaps. 4, 5 and 7, parameters in these models are descriptive by capturing the essence of a time-series data based on a disease outbreak. Although they may not carry any scientific hypotheses regarding the transmission dynamics, they provide an approach to investigate empirical patterns in observed data (Chowell et al. 2016).

In addition, we choose these simple models because

1. most of the transmission dynamic models defined by systems of differential equations do not have explicit solutions;
2. most of the numeric solutions of these equations can be closely approximated by one of the generalized logistic functions;
3. for those models that do have explicit solutions, they are either logistic or generalized logistic functions;
4. time-series data usually do not have sufficient information to identify the "mechanical assumptions" explicitly modeling the transmission dynamics.

8.2.1 The Sub-exponential Growth Function and the Generalized Growth Model (GGM)

This phenomenological model is useful to forecast epidemic growth patterns (Viboud et al. 2016; Chowell and Viboud 2016; Shanafelt et al. 2017; Pell et al. 2018a). In particular, previous analyses highlighted the presence of early sub-exponential growth patterns in infectious disease data across a diversity of disease outbreaks (Viboud et al. 2016).

The sub-exponential growth functions have been previously discussed in Sect. 4.5.2, in which we restricted our definition (4.56) as convex functions $C(t)$ bounded by the linear growth from below and the exponential growth from above, that is, $i_0\,(1 + rt) \leq C(t) \leq i_0 e^{rt}$. We have pointed out that the classic exponential growth function is associated with a set of strong mathematical assumptions and conditions when the system is at (disease-free) equilibrium, whereas during the initial stage of an outbreak in observed data, sub-exponential growth patterns are

more common. We have previously highlighted several mechanisms that potentially result in such growth patterns.

In particular, we consider the model $C(t) = i_0(1 + rvt)^{1/v}, 0 < v \leq 1$ for the cumulative incidence. If $v \to 0$, this model leads to the well-known exponential growth model, which applies both to the cumulative incidence $C(t)$ and to the instantaneous incidence $C'(t)$, while $v = 1$, corresponds to the linear growth of $C(t)$ and constant incidence per unit of time. $C(t) = i_0(1+rvt)^{1/v}, 0 < v \leq 1$, are illustrated in Fig. 4.11 in Chap. 4, as convex growth functions bounded by the linear growth and the exponential growth.

The generalized-growth model (4.61) in Viboud et al. (2016), which is also called the power law exponential model by Banks (1994), is defined by the differential equation

$$C'(t) = rC(t)^p, \ 0 \leq p \leq 1 \tag{8.1}$$

which allows relaxing the assumption of exponential growth via a "deceleration of growth" or "scaling of growth" parameter, p. $C'(t)$ describes the incidence growth phase over time t; the solution $C(t)$ describes the cumulative number of cases at time t.

When $i_0 = 1$ and letting $p = 1 - v$, the sub-exponential function $C(t) = (1 + rvt)^{1/v}$ is the solution of (4.61).

In semi-logarithmic scale, exponential growth patterns are visually evident when a straight line fits well several consecutive disease generations of epidemic growth, whereas a downward curvature in semi-logarithmic scale indicates early sub-exponential growth dynamics.

8.2.2 The Simple Logistic Function

In Chap. 5, we introduced many types of phenomenological models involving the dynamics of the process of interest (e.g., population or transmission dynamics). These types of models are often formulated in terms of a dynamic system describing the spatial-temporal evolution of a set of variables, and they are useful to evaluate the emergent behavior of the system across the relevant space of parameters (Chowell et al. 2016). In particular, compartmental models are based on systems of ordinary differential equations that focus on the dynamic progression of a population through different epidemiological states (Bailey 1975; Anderson and May 1991; Brauer 2006; Lee et al. 2016). While these models may not be useful for testing scientific hypotheses and formulating theory on disease transmission, they are very useful in practice such as for curve fitting, prediction as well as formulating of some statistical models, such as the back-calculation. One of the most memorable quotes from the wordsmith and former New York Yankees catcher, Yogi Berra, is:

> In theory, theory and practice are the same thing; in practice, they are different.

Several models, such as the SI model, the SIS model, and the model defined by (8.5), produce the logistic epidemiologic curves. Many other models also produce logistic-like epidemiologic curves that can be used to explain patterns in the observed data.

The logistic growth function (4.59) is one of the oldest growth functions with the following equivalent forms

$$C_{\text{logis}}(t) = \frac{i_0 K}{i_0 + (K - i_0)\, e^{-\rho t}} = \frac{K}{1 + \frac{1}{v} e^{-\rho t}} = \frac{K}{1 + e^{-\rho(t-\alpha)}} \tag{8.2}$$

where $v = \frac{i_0}{K - i_0}$ and $\alpha = \frac{1}{\rho} \log \frac{K - i_0}{i_0} = -\frac{1}{\rho} \log v$. In all these representations, there are three functionally independent parameters.

The logistic function was first proposed by Verhulst (1838). For modeling population growth, the logistic model was used and popularized by Pearl (1925), Pearl and Reed (1920), and Yule (1925). The expression

$$C_{\text{logis}}(t) = \frac{K}{1 + e^{-\rho(t-\alpha)}}, \quad -\infty < t, \alpha < \infty, \ \rho, K > 0. \tag{8.3}$$

characterizes the time-series data. The parameters (ρ, α, K) are descriptive about the general shape and are useful to fit to time-series data, of which ρ is the scale parameter associated with the initial growth; α is a location parameter that is also the inflexion point at which the increase of $C_{\text{logis}}(t)$ turns from convex to concave; $K = \lim_{t \to \infty} C(t)$ is the upper limit, referred to as the carrying capacity.

Many infectious disease models lead to the exact logistic growth form or growth functions very closely resembling logistic growth.

The deterministic SIS model produces the logistic function (5.14) for the number of infectious individuals at time t, as

$$I_d(t) = \frac{m i_0 (\beta - \gamma)}{\beta i_0 + (m(\beta - \gamma) - \beta i_0)\, e^{-(\beta - \gamma)t}}. \tag{8.4}$$

If $\beta - \gamma > 0$, $I_d(t)$ increases monotonically and approaches the value $m(1 - \gamma/\beta)$. It is the same as logistic function (4.59) via re-parametrization $K = m(1 - \gamma/\beta)$ and $\rho = \beta - \gamma$. Although in (8.4), the parameters (m, i_0, β, γ) are associated with hypotheses about the transmission dynamic, from the perspective of fitting the model to data, $I_d(t)$ only has three independent parameters. In fact, the time-series data that fit well with the logistic function do not have the information to test the hypothesis H_0: $\gamma = 0$ in the SIS model.

The logistic function can also arise from other deterministic transmission models. Tan (2000) considered the following compartment model

$$\begin{cases} \frac{d}{dt} S_d(t) = -\beta \frac{S_d(t) I_d(t)}{S_d(t) + I_d(t)} \\ \frac{d}{dt} I_d(t) = \beta \frac{S_d(t) I_d(t)}{S_d(t) + I_d(t)} - \gamma I_d(t) \\ \frac{d}{dt} Z_d(t) = \gamma I_d(t) - \delta Z_d(t) \end{cases}, \tag{8.5}$$

where $S_d(t)$ and $I_d(t)$, as in the SIS and SIR models, represent the numbers of susceptible and infected individuals in the population. The main difference from the deterministic models discussed before is that, in this model, all infectious individuals will progress to Compartment Z. Once individuals enter Compartment Z, they no longer make contacts with susceptible individuals. For instance, Compartment Z may represent advanced illness or being isolated. Thus the instantaneous infection function is modified as $\beta \frac{S_d(t) I_d(t)}{S_d(t)+I_d(t)}$.

Let $\psi(t) = \frac{I_d(t)}{S_d(t)+I_d(t)}$ be the proportion of infected individuals before entering Compartment Z, we have

$$\frac{d}{dt}\left[S_d(t) + I_d(t)\right] = -\gamma I_d(t) = -\gamma \psi(t)\left[S_d(t) + I_d(t)\right],$$
$$\frac{1}{S_d(t) + I_d(t)} \frac{d}{dt} I_d(t) = \psi(t)\left\{\left[1 - \psi(t)\right]\beta - \gamma\right\}.$$

It follows that

$$\begin{aligned}\frac{d}{dt}\psi(t) &= \frac{\left[S_d(t) + I_d(t)\right]\frac{d}{dt} I_d(t) - I_d(t)\frac{d}{dt}\left[S_d(t) + I_d(t)\right]}{\left[S_d(t) + I_d(t)\right]^2} \\ &= \frac{1}{S_d(t) + I_d(t)}\left\{\frac{d}{dt} I_d(t) - \psi(t)\frac{d}{dt}\left[S_d(t) + I_d(t)\right]\right\} \\ &= \rho\psi(t)\left[1 - \psi(t)\right],\end{aligned}$$

where $\rho = \beta - \gamma$. Clearly, $\psi(t)$ follows the logistic growth given by

$$\psi(t) = \frac{\psi(0)}{\psi(0) + \left[1 - \psi(0)\right] e^{-\rho t}}$$

and $\psi(t) \to 1$ as $t \to \infty$.

8.2.3 *Generalized Logistic Functions*

The logistic differential equation

$$\frac{d}{dt} C(t) = \rho K \left(\frac{C(t)}{K}\right)\left(1 - \frac{C(t)}{K}\right)$$

assumes that the per capita growth rate decreases linearly with population size or density. Its solution is the logistic function $C_{\text{logis}}(t) = \frac{i_0 K}{i_0 + (K - i_0) e^{-\rho t}}$ which can be also expressed as

$$C_{\text{logis}}(t;\rho,\alpha,K) = \frac{K}{1+e^{-\rho(t-\alpha)}}, \tag{8.6}$$

$$= K\left(1-\frac{1}{1+e^{\rho(t-\alpha)}}\right), \tag{8.7}$$

where $-\infty < t < \infty$ with three parameters (ρ, K, α): $\rho > 0$ is the scale parameter, $-\infty < \alpha < \infty$ is a location parameter and $K = \lim_{t\to\infty} C(t) > 0$ is the carrying capacity. It is symmetric in the sense that α is also the inflexion point at which $C_{\text{logis}}(\alpha) = K/2$. Given K and the initial value $i_0 = C_{\text{logis}}(0)$, $\alpha = \frac{1}{\rho}\log\frac{K-i_0}{i_0}$.

The first derivative $\frac{d}{dt}C_{\text{logis}}(t)$ is

$$I_{\text{logis}}(t) = \frac{d}{dt}C_{\text{logis}}(t) = \frac{ke^{-\rho(t-\alpha)}}{\left(1+e^{-\rho(t-\alpha)}\right)^2},$$

where $k = \rho K$. It reaches the maximum value at $t = \alpha$ such that $I_{\text{logis}}(\alpha) = \frac{k}{4}$. Meanwhile, $\lim_{t\to\infty} I_{\text{logis}}(t) = 0$.

The logistic function may be generalized in two directions: (1) asymmetric function for $I(t)$ by adding a shape parameter $\theta > 0$; (2) $\lim_{t\to\infty} I(t) = c > 0$, where $I(t) = \frac{d}{dt}C(t)$. A further generalization is to combine (1) and (2) to obtain more flexible forms in order to fit empirical data, especially for diseases with apparent endemic equilibrium. These will be discussed below.

Generalization Towards Asymmetry: The Richards Model and Its Variations

The symmetric shape of the logistic function makes it inflexible to fit data suggesting asymmetry. There are different ways to create asymmetric generalized logistic forms, such as

$$I_{\text{Glogis}}(t) = \frac{1}{1+e^{-\rho(t-\alpha)}}\frac{ke^{-\eta(t-\alpha)}}{1+e^{-\eta(t-\alpha)}}$$

where $\eta > 0$ may be different from the initial growth rate ρ. In this generalization, both parameters η and ρ act as scale parameters of time. It is inconvenient to interpret a model representing a time-series with two different scale parameters. In addition, it does not correspond to the generalization of the logistic differential equation.

The Richards growth curve (Richards 1959) is one of the best known generalized logistic functions. It adds a shape parameter $\theta > 0$ to scale the proportion $C(t)/K$ in the logistic differential equation. The result is the theta-logistic equation

$$\frac{d}{dt}C(t) = rK\left(\frac{C(t)}{K}\right)\left(1-\left[\frac{C(t)}{K}\right]^{\theta}\right),\ \theta > 0. \tag{8.8}$$

Causton and Venus (1981) show that, when $r > 0$ and $\theta > 0$, given $C(0) = i_0$,

$$C_{\text{Richards}}(t) = \frac{K}{\left(1 + Qe^{-r\theta t}\right)^{1/\theta}}, \tag{8.9}$$

where $Q = \left(\frac{K}{i_0}\right)^{\theta} - 1$. If we re-parameterize the scale parameter $\rho = r\theta$ and let $Q = e^{\rho\alpha}$, (8.9) becomes the following generalized logistic growth function

$$C_{\text{Richards}}(t; \rho, \alpha, \theta, K) = \frac{K}{\left[1 + e^{-\rho(t-\alpha)}\right]^{1/\theta}}, \tag{8.10}$$

which is directly adding the shape parameter into (8.6). In (8.10), $\rho, \theta, K > 0$ and $-\infty < \alpha < \infty$.

The first derivative $\frac{d}{dt}C_{\text{Richards}}(t)$ is

$$I_{\text{Richards}}(t) = \frac{ke^{-\rho(t-\alpha)}}{\left[1 + e^{-\rho(t-\alpha)}\right]^{\frac{\theta+1}{\theta}}} \tag{8.11}$$

where $k = \frac{\rho}{\theta}K$.

The inflexion point for $C_{\text{Richards}}(t)$ is

$$t^* = \frac{1}{r\theta}\left(\ln\frac{Q}{\theta}\right) = \alpha - \frac{1}{\rho}\log\theta.$$

At the inflexion point, $C_{\text{Richards}}(t^*) = \frac{K}{(1+\theta)^{1/\theta}}$. When $\theta < 1$, $C_{\text{Richards}}(t^*) < K/2$; when $\theta = 1$, $C_{\text{Richards}}(t^*) = K/2$ and when $\theta > 1$, $C_{\text{Richards}}(t^*) > K/2$. At the inflexion point, $I_{\text{Richards}}(t)$ arrives at the peak value $I_{\text{Richards}}(t^*) = \frac{\rho K}{(1+\theta)^{\frac{\theta+1}{\theta}}}$.

The Richards model has been fitted to a range of epidemic curves that exhibit sigmoid cumulative growth patterns (Turner et al. 1976; Ma et al. 2014; Wang et al. 2012; Hsieh and Cheng 2006; Dinh et al. 2016).

A Variation of the Richards Model Instead of adding the shape parameter θ into (8.6), we add it into (8.7) and we get the generalized logistic growth function

$$C_{\text{Richards2}}(t; K, \rho, \alpha, \theta) = K\left(1 - \frac{1}{\left[1 + e^{\rho(t-\alpha)}\right]^{1/\theta}}\right), \quad K, \rho, \alpha, \theta > 0. \tag{8.12}$$

Both generalized logistic functions are related through

$$C_{\text{Richards2}}(t; K, \rho, \alpha, \theta) = K - C_{\text{Richards}}(-t; K, \rho, -\alpha, \theta).$$

It can be easily shown that (8.12) is the solution of the theta-logistic equation

$$\frac{d}{dt}C(t) = rK\left(1 - \left[1 - \frac{C(t)}{K}\right]^{\theta}\right)\left(1 - \frac{C(t)}{K}\right),\ \theta > 0 \tag{8.13}$$

with

$$C_{\text{Richards2}}(t) = K\left(1 - \frac{1}{\left[1 + Q_2 e^{r\theta t}\right]^{1/\theta}}\right) \tag{8.14}$$

where $Q_2 = \left(\frac{K}{K-i_0}\right)^{\theta} - 1$. Clearly, $C_{\text{Richards2}}(t)$ in (8.14) and in (8.12) is the same, via re-parametrization $\rho = r\theta$ and $Q_2 = e^{-\rho\alpha}$.

The first derivative $\frac{d}{dt}C_{\text{Richards2}}(t)$ is

$$I_{\text{Richards2}}(t) = \frac{ke^{\rho(t-\alpha_2)}}{\left[1 + e^{\rho(t-\alpha_2)}\right]^{\frac{\theta+1}{\theta}}} \tag{8.15}$$

where $k = \frac{\rho}{\theta}K$.

If the initial value i_0, the scale parameter ρ, the shape parameter θ, and the carrying capacity K are all the same in both (8.10) and (8.12), the location parameter α in the corresponding solutions (8.10) and (8.12) is different. We denote them separately as α_1 and α_2, respectively. They are

$$\begin{aligned}
\alpha_1 &= \tfrac{1}{\rho}\log\left[\left(\tfrac{K}{i_0}\right)^{\theta} - 1\right], && \text{with respect to (8.9)}\\
\alpha_2 &= -\tfrac{1}{\rho}\log\left[\left(\tfrac{K}{K-i_0}\right)^{\theta} - 1\right], && \text{with respect to (8.14).}
\end{aligned}$$

The inflexion point for $C_{\text{Richards2}}(t)$ is $t_2^* = \alpha_2 + \frac{1}{\rho}\log\theta$ and $C_{\text{Richards2}}(t_2^*) = K\left(1 - \frac{1}{(1+\theta)^{1/\theta}}\right)$. At the inflexion point, $I_{\text{Richards2}}(t)$ reaches the peak value $I_{\text{Richards2}}(t_2^*) = \frac{\rho K}{(1+\theta)^{\frac{\theta+1}{\theta}}}$ which is the same as the peak value of $I_{\text{Richards}}(t)$.

Figure 8.1 compares $C_{\text{Richards}}(t)$ vs. $C_{\text{Richards2}}(t)$, and $I_{\text{Richards}}(t)$ vs. $I_{\text{Richards2}}(t)$, given $K = 1000$, $i_0 = 1$ and $\theta = 0.4$. Since ρ is a scale parameter with respect to time, without losing generality, we let $\rho = 1$. We have

$$\begin{aligned}
\alpha_1 &= 2.6979,\ t_1^* = 2.6979 - \log 0.4 = 3.6142\\
\alpha_2 &= 7.8233,\ t_2^* = 7.8233 + \log 0.4 = 6.907
\end{aligned}$$

and $I_{\text{Glogis1}}(t_1^*) = I_{\text{Glogis2}}(t_2^*) = 308$.

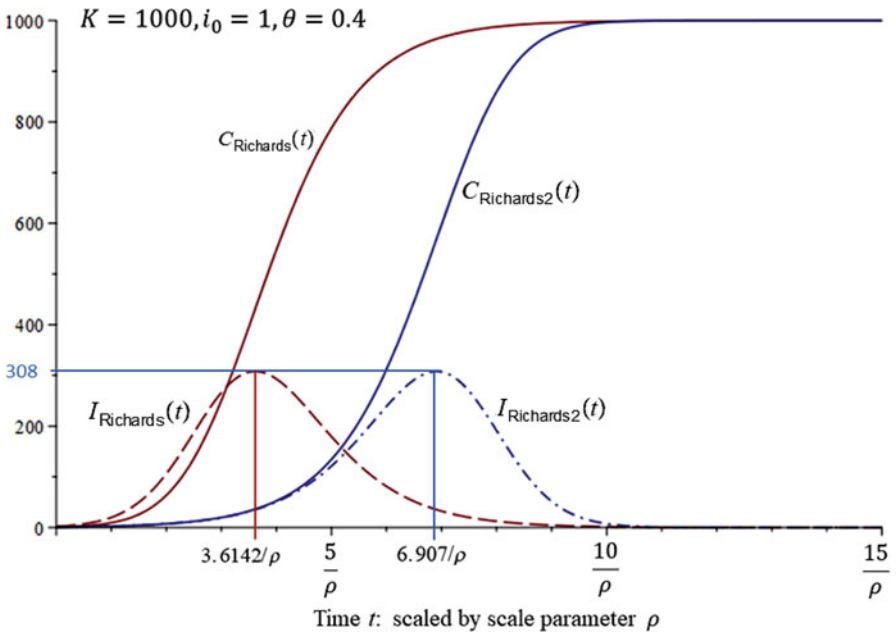

Fig. 8.1 Plots of $C_{\text{Richards}}(t)$, $I_{\text{Richards}}(t)$, $C_{\text{Richards2}}(t)$, and $I_{\text{Richards2}}(t)$ given $K = 1000$, $i_0 = 1$, $\theta = 0.4$. The time scale is standardized according to the scale parameter ρ. The maximum values for $I_{\text{Richards}}(t)$ and $I_{\text{Richards2}}(t)$ are equal: $\rho K\,(1+\theta)^{-\frac{\theta+1}{\theta}} = 308$ at set parameters

The variation of the Richards model (8.12) is closely related to disease transmission model (8.5). In (8.5), $\psi(t) = \frac{I_d(t)}{S_d(t)+I_d(t)}$ is a simple logistic growth function. However, $I_d(t)$ in (8.5) is an asymmetric bell-shaped curve

$$I_d(t) = M(0)\frac{\psi(0)e^{\rho t}}{\{[1-\psi(0)]+\psi(0)e^{\rho t}\}^{1+\gamma/\rho}}, \tag{8.16}$$

where $M(0) = S_d(0) + I_d(0)$. If we re-parameterize $\theta = \rho/\gamma$ and $\psi(0) = \left(\frac{K}{K-i_0}\right)^{\theta} - 1 \equiv Q_2$, then (8.16) becomes

$$I_d(t) = M(0)\frac{Q_2 e^{\rho t}}{\left\{\left(\frac{K}{K-i_0}\right)^{\theta} + Q_2 e^{\rho t}\right\}^{\frac{\theta+1}{\theta}}}.$$

On the other hand, (8.15) with re-parametrization is

$$I_{\text{Richards2}}(t) = k\frac{Q_2 e^{\rho t}}{\{1+Q_2 e^{\rho t}\}^{\frac{\theta+1}{\theta}}}.$$

Thus $I_{\text{Richards2}}(t)$ approximates $I_d(t)$ in (8.16) well when K is large and i_0 is small.

The model given by (8.15) is descriptive and captures the essence of time-series data based on a disease outbreak without any scientific hypothesis regarding the transmission dynamics. It has been used as approximations for some simple compartment models for HIV/AIDS, as discussed in detail in Chap. 9 of Brookmeyer and Gail (1994) and Chap. 1 of Tan (2000).

The following example illustrates the generalized logistic functions (8.12) and (8.15) as good approximations to two different SIR-type models and an SEIR model.

Example 33 In this example, we set $K = 9009$, $\alpha = 53.46$, $\varphi = 0.72$, $\rho = 0.155$ in (8.15). The parameter $\varphi = 0.72 < 1$ gives a slightly skewed incidence function $I_d(t)$ with peak time $t^* = 55.579$. According to this model, the final size is $C(\infty) = 9009$. Both (8.12) and (8.15) approximate very well with the incidence and cumulative incidence functions, which are implicitly determined by the following selected deterministic models (Fig. 8.2):

1. the SIR model given by (5.24) with $m = S(0) + I(0) = 14{,}300$, $\beta = 0.395$, $\gamma = 1/4$, corresponding to $R_0 = 1.58$ and final size 9025;
2. the SEIR model given by (5.53) with $m = S(0) + I(0) = 10{,}150$, $\beta = 0.6$, $\alpha = 1/3.4$, $\gamma = 1/4$, corresponding to $R_0 = 2.4$ and final size 8918;
3. an SIR model governed by the integro-differential equations

$$\begin{cases} \frac{d}{dt}S(t) = -\beta\frac{S(t)I(t)}{n} \\ \frac{d}{dt}I(t) = i(t) - \int_0^t i(s)f_I(t-s)ds, \text{ where } i(t) = \beta\frac{S(t)I(t)}{n} \\ \frac{d}{dt}R(t) = \int_0^t i_1(s)f_I(t-s)ds. \end{cases}$$

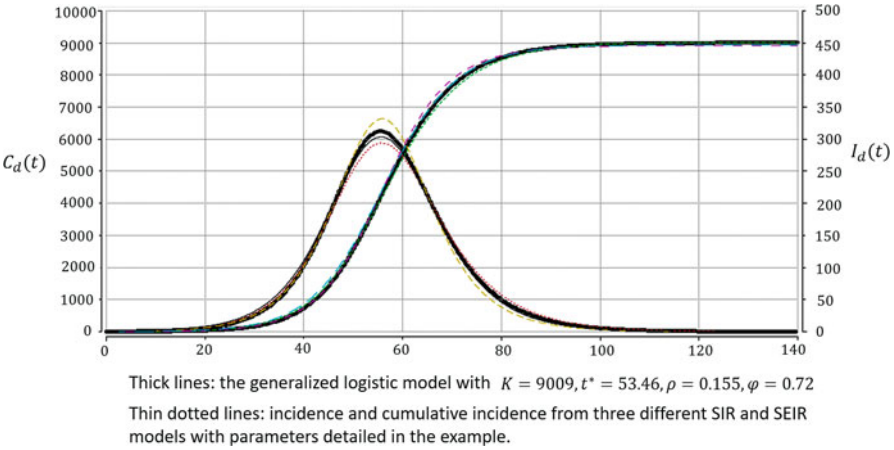

Fig. 8.2 Illustration of generalized logistic models $C_d(t)$ and $i_d(t)$ with comparison from three different transmission models in Example 33

with gamma distributed infectious period $f_I(x)$ with mean value $\mu_I = 4$ and shape parameter $\kappa = 3$, along with $m = S(0) + I(0) = 17{,}500$, $\beta = 0.35$, corresponding to $R_0 = 1.4$ and final size 8945.

Other Variations and Generalizations An alternative to (8.13) is

$$\frac{d}{dt}C(t) = rK\left[\frac{C(t)}{K}\right]^{\theta}\left(1 - \frac{C(t)}{K}\right), \tag{8.17}$$

Although it looks much simpler than (8.13), there is no explicit solution, but $C(t)$ can be solved numerically. It is also a sigmoid growth function with an inflexion point t^* at which $C(t^*) = \frac{p}{p+1}K$.

Other variations include

$$\frac{d}{dt}C(t) = r\left[C(t)\right]^{\theta}\left(1 - \frac{C(t)}{K}\right), \tag{8.18}$$

or the generalized Richards model (Turner et al. 1976) with two shape parameters $\theta_1, \theta_2 > 0$:

$$\frac{d}{dt}C(t) = r\left[C(t)\right]^{\theta_1}\left(1 - \left[\frac{C(t)}{K}\right]^{\theta_2}\right). \tag{8.19}$$

The model (8.19) with $0 < \theta_1 \leq 1$ was used to account for initial sub-exponential growth dynamics (Viboud et al. 2016). In this case, θ_1 is called the "deceleration of growth" parameter. This model has been useful to generate post-peak forecasts of Zika and Ebola epidemics (Pell et al. 2018a; Chowell et al. 2016).

Generalizations of the Logistic and Richards Functions So That $\lim_{t\to\infty} I(t) = c > 0$

It is straightforward to generalize $I_{\text{logis}}(t)$ into

$$I_{\text{logis-c}}(t) = \frac{1}{1 + e^{-\rho(t-\alpha)}}\left(\frac{ke^{-\rho(t-\alpha)}}{1 + e^{-\rho(t-\alpha)}} + c\right). \tag{8.20}$$

It returns to the logistic model when $c = 0$. However, $I_{\text{logis-c}}(\alpha)$ is not the maximum value unless $c = 0$ because $I'_{\text{logis-c}}(\alpha) = \frac{1}{4}c\rho \geq 0$. The maximum value is achieved when $t = t^* = \alpha - \frac{1}{\rho}\log\frac{k-c}{k+c}$ and the maximum value is $I_{\text{logis-c}}(t^*) = \frac{1}{4k}(k+c)^2$.

Similarly, one can generalize the Richards function (8.11) as

$$I_{\text{Richards-c}}(t) = \frac{1}{1 + e^{-\rho(t-\alpha)}}\left(\frac{ke^{-\rho(t-\alpha)}}{\left[1 + e^{-\rho(t-\alpha)}\right]^{\frac{1}{\theta}}} + c\right) \tag{8.21}$$

that includes five parameters. It returns to the Richards model (8.11) when $c = 0$; returns to (8.20) when $\theta = 1$ and returns to the logistic model when $c = 0$ and $\theta = 1$. It satisfies $I_{\text{Richards-c}}(-\infty) = 0$ and $I_{\text{Richards-c}}(\infty) = c \geq 0$. It reaches the peak value when $t = t^*$ that satisfies

$$ke^{-\rho(t-\alpha)} + c\theta\left(e^{-\rho(t-\alpha)} + 1\right)^{\frac{1}{\theta}} = k\theta.$$

For the special cases, $t^* = \alpha$ when $c = 0$ and $\theta = 1$; $t^* = \alpha - \frac{1}{\rho}\log\theta$ when $c = 0$ and $t^* = \alpha - \frac{1}{\rho}\log\frac{k-c}{k+c}$ when $\theta = 1$.

A different generalization of (8.20) is

$$I_{\text{logis-c-2}}(t) = \frac{1}{1 + e^{-\rho(t-\alpha)}}\left[\frac{ke^{-\eta(t-\alpha)}}{1 + e^{-\eta(t-\alpha)}} + c\right] \tag{8.22}$$

where

ρ = rate of increase at the beginning,
η = rate of convergence to the asymptote.
a = a suitable location parameter,
$c = \lim_{t\to\infty} I_{\text{logis-c-2}}(t)$ = asymptote.

The generalized logistic function given by (8.22) has been adopted as one of the parametric models for the incidence of new HIV infections in a computer package, Spectrum (Avenir Health), which is endorsed by the Joint United Nations Programme on HIV/AIDS (UNAIDS) to compile estimates of HIV prevalence in different countries around the world.

Both (8.21) and (8.22) have five parameters. They may be used to approximate SEIRS models in a constant population with demography turn-over. A comparison is shown in Fig. 8.3. However, it is inconvenient to interpret the model (8.22) representing a time-series with two different scale parameters, η and ρ.

These generalized logistic functions can be used to capture the essence of time-series data for prediction purposes. By adding more parameters, one can create models that can capture a broad variety of epidemic curves. For example, the following 6-parameter function

$$I_{twin-peak-c}(t) = \frac{k_1 e^{-\rho(t-\alpha_1)}}{(1 + e^{-\rho(t-\alpha_1)})^2} + \frac{1}{1 + e^{-\rho(t-\alpha_2)}}\left[\frac{k_2 e^{-\rho(t-\alpha_2)}}{1 + e^{-\rho(t-\alpha_2)}} + c\right]$$

is capable of creating a twin peaked curve that approaches an asymptote $c > 0$. However, the time-series data, especially data from a single source, do not have enough information to test hypotheses or make statistical inferences on parameters with specific biological and epidemiological interpretations in transmission models.

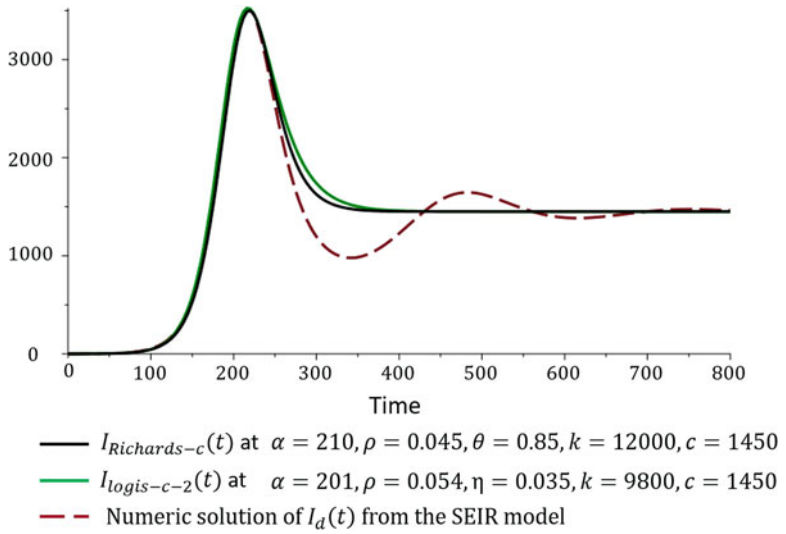

Fig. 8.3 Compare the functions (8.21) and (8.22) with selected parameters against the numbers of infectious individuals over time in an SEIRS model using parameters in Example 25 (dashed line)

8.3 A Comprehensive Demonstration of Curve Fitting Using Nonlinear Phenomenological Models to Outbreak Data from the 2016 Zika Epidemic in Antioquia, Colombia

In the Western Hemisphere, active circulation of ZIKV was first reported in Brazil in May 2015, and the WHO declared the epidemic a Public Health Emergency of International Concern on February 1, 2016. Phylogenetic analyses indicate that the epidemic in the Americas was triggered by an imported case sometime between May and December 2013, a period that coincides with an increase in air travel from ZIKV affected areas in the Pacific to Brazil (Faria et al. 2016).

We analyzed daily counts of Zika cases by date of symptoms onset reported to the Secretary of Health of Antioquia (the time series is available online as an EXTRA MATERIAL). Antioquia is the second largest department in Colombia (with a population size of ~6.3 million people), located in the central northwestern part of the country (Chowell et al. 2016). Because there is still substantial uncertainty on the epidemiology of ZIKV, including the contribution of different modes of transmission (mosquito bites vs. sexual transmission), simple phenomenological models are useful for forecasting epidemic trajectories whereas mechanistic mosquito-borne disease transmission models require more data to appropriately calibrate mosquito reproduction, development, survival, and transmission capacity which are strongly modulated by temperature as well as the transmission rates that dictates the transfer of the virus from mosquitoes to humans and vice versa (e.g., Ross 1911; Focks et al. 1995; Chowell et al. 2007; Gao et al. 2016; Towers et al. 2016; Zhang et al. 2017; Huber et al. 2018).

8.3.1 Fitting Models to Data

The time-series data $\underline{y} = (y_0, y_1, \ldots, y_T)$ represent daily incidence according to the onset of clinical symptoms. The date of the earliest recorded case by date of onset is called Day 0. We model the cumulative number of clinical cases by time t according to a counting process. The random component of the model is the marginal distribution of $C(t)$ grouped into time intervals so that $Y_t = C(t) - C(t-1)$, $-\infty < t < \infty$ is the number of clinical onsets during the time interval $(t-1, t]$. The systematic component of the model is a deterministic growth curve function $C_d(t)$, chosen as one of the growth curve functions introduced in the preceding section, such that the expected value is $E[C(t)] = C_d(t)$, specified by a set of parameters $\Theta = (\theta_1, \ldots, \theta_m)$.

Since we are fitting the model to daily incidence data y_t, we write the systematic component as

$$\mu(t; \Theta) = C_d(t) - C_d(t-1).$$

Most of the growth functions are defined over $-\infty < t < \infty$. Therefore the expected number of new cases by date of symptoms on Day 0 is $E[Y_0] = \mu(0; \Theta) = C_d(0) - C_d(-1)$. In the observed data, $y_0 = 1$.

We use the methods presented and discussed in Sect. 7.1.3 in the following analyses.

8.3.2 Data During the First 20 Days

Exploratory Analysis

Starting from the earliest recorded case by date of onset, denoted as Day 0, the cumulative number of confirmed individuals with clinical symptoms was 183 by Day 20. During the first 2 weeks, daily incidence numbers by symptoms onset were rather sporadic, less than 10 cases per day except for Day 9 and Day 14. From Day 15 to Day 20, the daily incidence numbers were fluctuating between 12 and 20 cases per day.

Exploratory plots of the logarithm of daily incidence data $(y_t,\ t = 0, \ldots, 20)$ against time t and against the logarithm of the cumulative incidence $c_t = \sum_{i=0}^{t} y_i$, $t = 0, \ldots, 20$ (Fig. 8.4) show distinctive sub-exponential growth patterns. In particular, the strong linear relationship between the logarithm of daily incidence data and the logarithm of the cumulative incidence is given by

$$\log y_t = -0.06008 + 0.55466 \log \sum_{i=0}^{t} y_i,$$

which empirically agrees with the relationship $C'(t) = rC(t)^p$, in which, $C'(t)$ is approximated by the daily incidence y_t, $t = 1, \ldots, 20$ and $y_0 = 1$ and $C(t)$ is

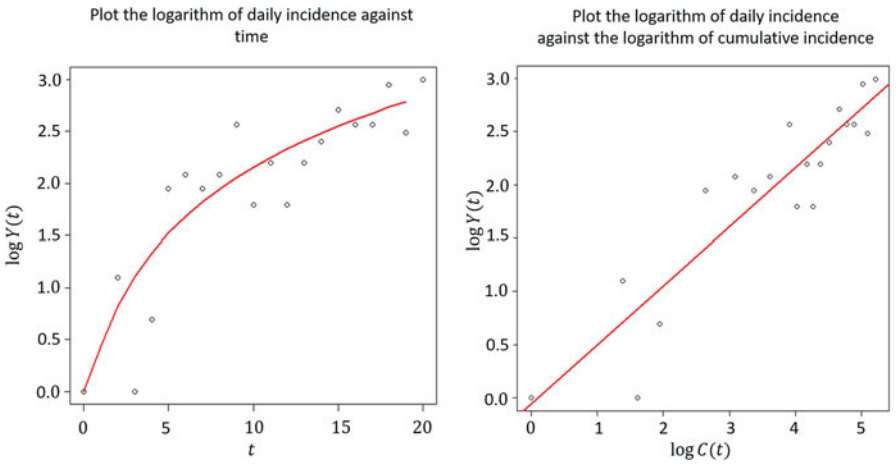

Fig. 8.4 Exploratory plots of the logarithm of daily incidence data $\log y_t$ against time t and against the cumulative incidence $c_t = \sum_{i=0}^{t} y_i$, $t = 0, .., 20$

approximated by the cumulative incidence $c_t = \sum_{i=0}^{t} y_i$. This relationship gives the crude estimates

$$\widetilde{r} = e^{-0.06008} = 0.94169, \ \widetilde{p} = 0.55466.$$

Likelihood Analysis, Estimation and Predictions for the Sub-exponential Model

For formal analysis, we start fitting to daily incidence data using (7.3), assuming that $\underline{y} = (y_0, y_1, \ldots, y_{20})$ are realizations of independent Poisson random counts. The likelihood based approach based on (7.4) is applied with $f(0; \Theta) = i_0$ and $f(t; \Theta) = C(t) - C(t-1)$, $t = 1, \ldots, 20$, where $C(t) = i_0(1 + r(1-p)t)^{\frac{1}{1-p}}$, $0 \leq p < 1$.

We first conduct the likelihood ratio test against the hypothesis $H_0 : i_0 = 1$, which yields a significant level (p-value) of 0.48. There is no evidence from data to reject H_0.

We consider the reduced model $C(t) = (1 + r(1-p)t)^{\frac{1}{1-p}}$, which is the exact solution of $C'(t) = rC(t)^p$ given the initial condition $C(0) = 1$. The parameters are $\Theta = (r, p)$. The maximum likelihood estimates are

$$\widehat{r} = 1.172 \ (0.8173, 1.777)$$

$$\widehat{p} = 0.5189 \ (0.4231, 0.6186)$$

where numbers in brackets are 95% confidence limits calculated using likelihood ratio statistics.

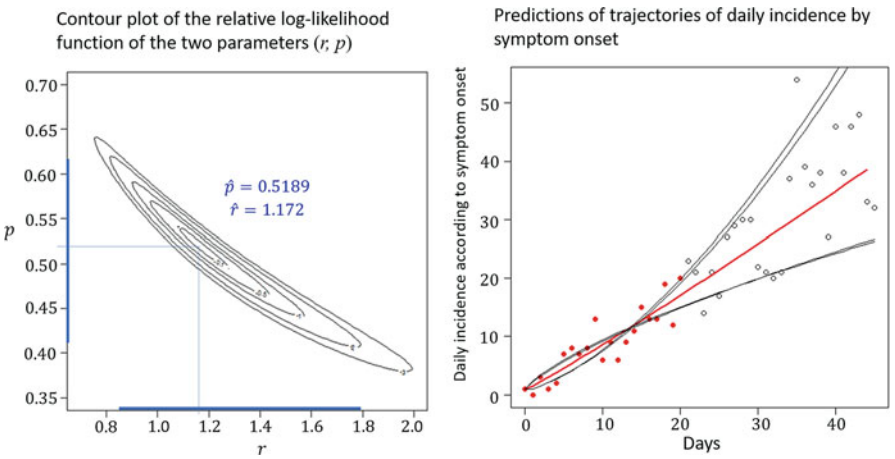

Fig. 8.5 Left: the contours of the relative log-likelihood function for (r, p) in the neighborhood of $(\widehat{r}, \widehat{p})$. Right: five predicted trajectories of daily incidence of onset of symptoms to Day 45. Red dots represent data from the first 20 days and circles are data from Day 21 to Day 45

One of the advantages of using the likelihood based approach is that the likelihood function reveals how much information data contain with respect to each of the parameters as well as correlations among parameters. Figure 8.5 (left) displays the contours of the relative log-likelihood function for (r, p) in the neighborhood of the maximum likelihood estimates. It shows substantial correlation due to the "banana" shape of the log-likelihood contour. Although the 95% confidence interval for each parameter has been calculated marginally for each parameter, not all the combinations of the two parameters within their ranges are plausible. For example, it is very implausible to have the combination $(r_L = 0.8173,\ p_L = 0.4231)$. This leads to the concept of the "profile likelihood," which is to fix one of the parameters at a given value and conduct a likelihood analysis on the rest of the parameters.

- Keeping r fixed at its lower bound at $r_L = 0.8173$, the profile likelihood for p is maximized at $\widehat{p}(r = 0.8173) = 0.6167$.
- Keeping r fixed at its upper bound at $r_U = 1.777$, the profile likelihood for p is maximized at $\widehat{p}(r = 1.777) = 0.411$.
- Keeping p fixed at its lower bound at $p_L = 0.4231$, the profile likelihood for r is maximized at $\widehat{r}(p = 0.4231) = 1.6693$.
- Keeping p fixed at its upper bound at $p_U = 0.6186$, the profile likelihood for r is maximized at $\widehat{r}(p = 0.6186) = 0.8222$.

Short term predictions may be conducted in ad hoc manner by simple extrapolation based on the model $f(t; \Theta)$ and the range of uncertainties in estimated parameters. Figure 8.5 (right) displays five predicted trajectories of daily incidence of onset of symptoms to Day 45 based on observed data up to Day 20. The center red line is the predicted trajectory based on the m.l.e. $(\widehat{r} = 1.172,\ \widehat{p} = 0.5189)$. The four

thin dark lines are predicted trajectories based on the combinations: $r = 0.8173$ and $p = 0.6167$; $r = 1.777$ and $p = 0.411$; $r = 1.6693$ and $p = 0.4231$; $r = 0.8222$ and $p = 0.6186$.

A word of caution is in place. Prediction of future trajectories based on historical data involves two sources of uncertainty: the uncertainty about the parameters and the uncertainty of future data due to randomness for any fixed parameter values in the probability distribution. The predictions in Fig. 8.5 (right) partially take into account the first source uncertainty but fail to take into account the second source. This issue is deeply rooted in the foundations of statistical inferences, and there is a scarcity of literature on "predictive likelihood" that is applicable to predicting trajectories of disease outbreaks.

Least Square Estimation and Predictions for the Sub-exponential Model

The least square method by minimizing (7.6) provides similar estimates

$$\widetilde{r} = 1.2023\ (0.76,\ 1.9)$$
$$\widetilde{p} = 0.5119\ (0.39,\ 0.64)$$

where numbers in brackets are 95% confidence limits based on 500 bootstrap samples, which are slightly wider than, but comparable to, those based on the likelihood ratio statistics.

Both the maximum likelihood estimates based on the Poisson distribution and the least square estimates are based on unbiased estimating equations. They are asymptotically unbiased point estimates regardless of any mis-specification of the variance–covariance structure. The word "asymptotic" is used in the sense of a large number of realizations of the same epidemic assuming the outbreak can be repeated under identical conditions. However, the point estimates in both methods are based on a single realization and are subject to biases.

For assessment of uncertainties, both methods are prone to mis-specification of the variance–covariance structure. In order to compare with the variance estimates based on the likelihood approach, 500 bootstrap replicates are generated for the least square estimation assuming a Poisson variance structure. Prediction intervals are also generated using bootstrapping to predict the distribution of individual future points.

The 95% confidence intervals for p based on both methods show strong significance against the hypothesis of the exponential growth function: $p \to 1$.

With respect to prediction of future trajectories, the bootstrapping method takes into account both sources of uncertainty. The cyan curves in Fig. 8.6 (right) correspond to 500 bootstrap replicates of the epidemic curve assuming a Poisson variance structure. These are predicted random numbers. The uncertainty in predicted trajectories is much larger than that in Fig. 8.5 (right). However, there are several issues worth discussing.

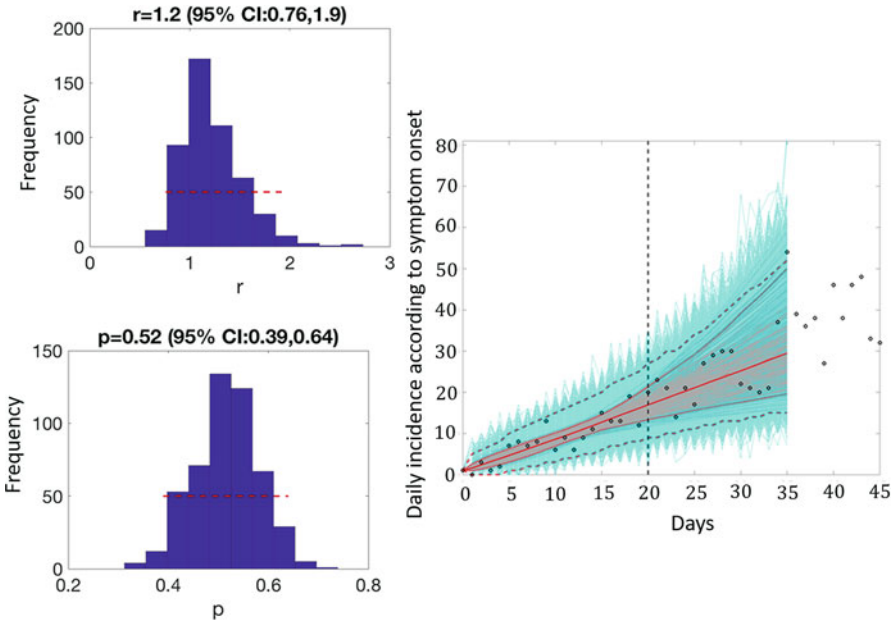

Fig. 8.6 Left: empirical distributions of the estimated parameters based on 500 bootstrap replicates. Right: 15-day forecast when the model is calibrated to the first 20 days. The black circles are the daily incidence data. The cyan curves correspond to 500 bootstrap replicates of the epidemic curve assuming a Poisson error structure. The red solid line corresponds to the asymptotic mean value of these replicates. The gray lines correspond to the fits of the model to each of the 500 bootstrap replicates from which 95% confidence intervals for the mean model fit can be derived (red dotted lines). The vertical line separates the calibration and forecasting periods

First, we note that the marginal distributions of the parameters (r, p) alone do not provide the insight as some of the combination of parameters (r, p) while $r \in (0.76, 1.9)$ and $p \in (0.39, 0.64)$ are highly implausible. Therefore, running simulations in these parameter ranges may produce larger than expected uncertainty. However, one could make use of the raw empirical distributions of the parameters including their correlations which were derived from the bootstrap approach in order to avoid selecting implausible parameter combinations.

Second, the vertical line separates the calibration and forecasting periods in Fig. 8.6 (right). The cyan curves correspond to 500 bootstrap replicates of the epidemic curve assuming a Poisson variance structure. They show large uncertainty in data that have already occurred. This is due to the virtual experiment conducted by the computer simulation assuming the outbreak can be repeated in identical conditions and the uncertainty in data reflects such randomness. However, the disease outbreak only occurs once and data in the past 20 days are given. Given past data, conditional prediction for the future is desirable whereas extrapolating "predictions" made for the past that include large uncertainty into the future is not desirable.

Fitting the Logistic Growth Model to the First 20 Epidemic Days of Data

Choosing the appropriate models and how to parameterize the models depends on what public health questions need to be addressed. For instance, public health officials may be less interested in short term predictions but more interested in questions such as

- Are the daily incidence numbers approaching the peak value?
- If this outbreak is going to be a single wave, how long is this wave expected to last?
- How many cumulative infections do we expect by the end of this wave?

Although sub-exponential growth (8.1) describes the growth pattern for the first 20 days of data and makes short-term predictions, it is unable to answer these questions. The logistic growth function characterizes such single wave phenomenon. The expression

$$C(t) = \frac{K}{1 + e^{-\rho(t-\alpha)}}$$

corresponds to the three questions, where the peak time is the location parameter α; the peak value of daily incidence is $C'(\alpha) = \rho K/4$ and by the end of the outbreak, the cumulative number of infected individuals is K. In addition, the logistic model is symmetric such that, at the peak time α, the cumulative incidence $C(\alpha) = K/2$.

For data $\underline{y} = (y_0, y_1, \ldots, y_{20})$, we specify the mean value $E[Y_t] = f(t; \Theta)$ where $f(t; \Theta) = C(t) - C(t-1)$ is the difference of the two adjacent cumulative values. Since the logistic model is defined for $-\infty < t < \infty$, $f(0; \Theta) = C(0) - C(-1)$ which is the expected value for Y_0.

The Likelihood Analysis The maximum likelihood estimates, assuming Poisson distribution for Y_t, are

$$\widehat{\rho} = 0.171 \ (0.092, \ 0.238)$$

$$\widehat{\alpha} = 19.71 \ (15.5, \ 45.8)$$

$$\widehat{K} = 377.898 \ (246, \ 4250)$$

where numbers in brackets are 95% confidence limits based on the likelihood ratio statistics. The very wide confidence limits show that data have little information about the key parameters of interest. The peak time could be anywhere from Day 15 to Day 46, and the total number of infections by the end of the wave could be anywhere between 246 and 4250.

Figure 8.7 illustrates cross-sectional contour plots for (α, K) according to selected growth rate values of ρ. Figure 8.7 shows that at a slow growth rate $\rho_L = 0.092$, the likelihood function suggests that the most plausible peak time occurs around Day 46, and by the end of the outbreak, the total number of infections would most likely be around 2500. However, there is a great deal of uncertainty

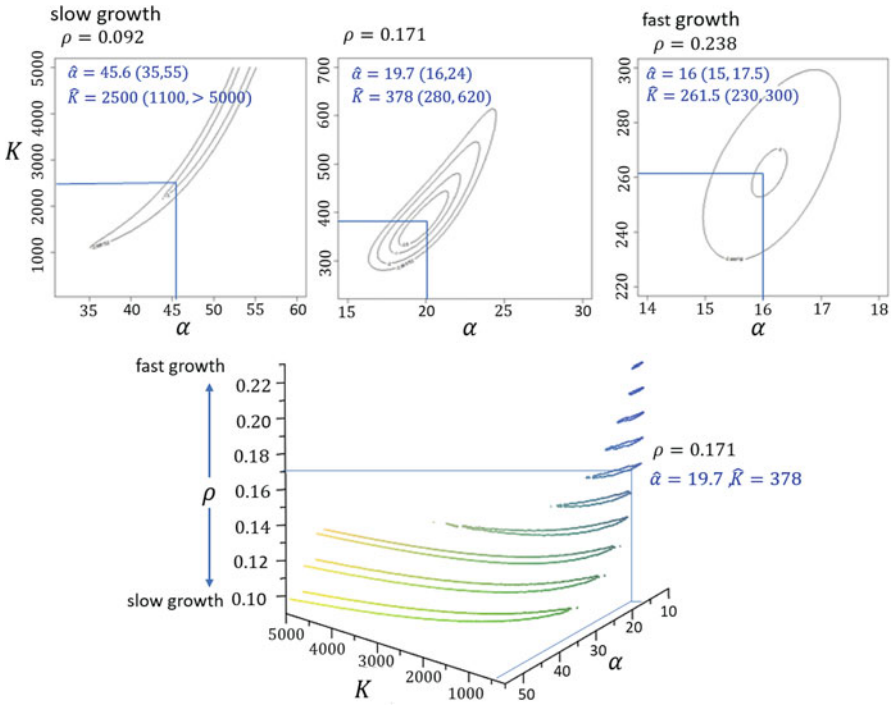

Fig. 8.7 Cross-sectional plots of the contours of the log-likelihood surface for (α, K) at $\rho = 0.092$, 0.171, and 0.238

suggesting that K could be as large as >5000. On the other hand, at a fast growth rate $\rho_H = 0.238$, the most plausible peak time occurs around Day 16, and the likelihood function predicts a small outbreak with the most plausible $K = 262$.

The logistic function can be also parameterized as

$$C(t) = \frac{K}{1 + e^{-\rho(t-\alpha)}} = \frac{i_0(v+1)}{v + e^{-\rho t}}$$

where $i_0 = C(0)$ is the cumulative number of clinical cases at time $t = 0$ and $v = e^{-\rho\alpha} = \frac{i_0}{K - i_0}$. The maximum likelihood estimates are

$$\widehat{\rho} = 0.171\ (0.092,\ 0.238)$$
$$\widehat{v} = 0.034\ (0.00001,\ 0.061)$$
$$\widehat{i_0} = 12.5\ (5.25,\ 39),$$

where numbers in brackets are 95% confidence limits based on the likelihood ratio statistics. Since data have little information about K, they equally have little information about v.

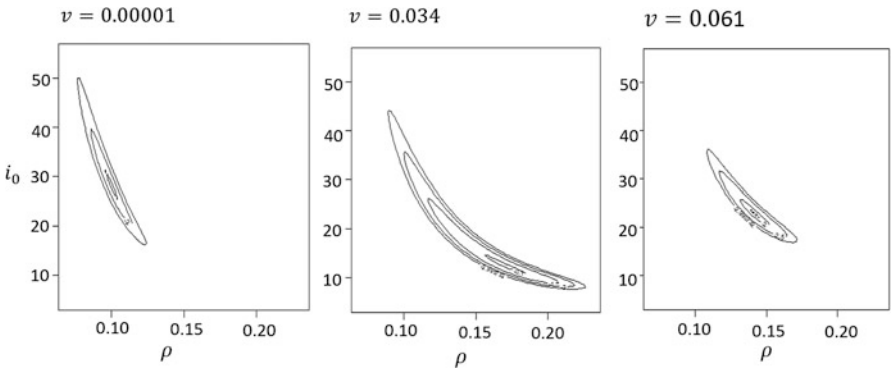

Fig. 8.8 Cross-sectional plots of the contours of the log-likelihood surface for (ρ, i_0) at $v = 0.00001$, 0.034, and 0.061

The logistic model suggests that on Day 0, the cumulative number $i_0 = C(0)$ was likely between 5 and 39, suggesting the outbreak might have started earlier. This estimated range, combined with the uncertainty estimates of the other parameters, suggests that the range of daily incidence on Day 0 might be in the range (1.1, 3.4). This is because the expected value for Y_0 is $f(0) = C(0) - C(-1)$. In the data, $y_0 = 1$.

Based on the contours of the log-likelihood (Fig. 8.8), the growth rate ρ is correlated with the initial cumulative number $i_0 = C(0)$. Although there was little information in the early data, we may tentatively make the following statements regarding the following three scenarios:

1. High cumulative numbers i_0 in the range between 30 and 40 (approximately three new clinical cases on Day 0) combined with slow growth $\rho < 0.1$. Under this scenario, it is likely that the peak time will be rather late, after Day 40. Consequently, the cumulative number by the end of the wave (assuming a single wave) might be above 2000, or even above 4000.
2. A plausible cumulative numbers i_0 around 12 (approximately two new clinical cases on Day 0) combined with a growth rate around 0.171. Although this scenario corresponds to the maximum likelihood, it is also likely to be biased, as it puts the estimated peak time at $\widehat{\alpha} = 19.71$ corresponding to the last data point ($t = 20$). There is no indication in data that the daily incidence is reaching its peak. If this were true, then the cumulative number by the end of the wave would be approximately twice the cumulative number at Day 20, which is 377.898.
3. Low cumulative numbers i_0 around 5 (approximately one new clinical case on Day 0) combined with a fast growth $\rho > 0.23$. This scenario may fit better for the very early part of the data, for instance, $t = 0, \ldots, 5$. However, there is no indication in data suggesting that the peak time has taken place before Day 20.

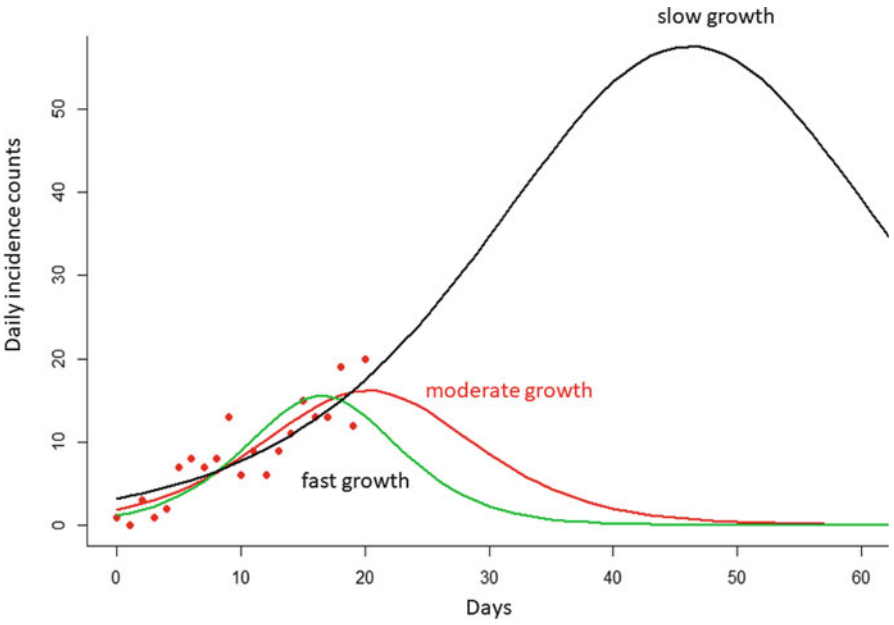

Fig. 8.9 Three predicted trajectories: (1) slow growth at $r = 0.092$, $\alpha = 45.6$ and $K = 2500$; (2) moderate growth at $r = 0.171$, $\alpha = 19.7$ and $K = 370$; (3) fast growth at $r = 0.238$, $\alpha = 16$ and $K = 262$

Figure 8.9 shows predictions to Day 60, with parameters chosen from the slow growth (with high i_0), moderate and fast growth patterns (with lower i_0). Data from the first 20 days cannot distinguish these scenarios.

We remark that the likelihood surfaces are highly asymmetric with respect to the parameters of interest. For example, the m.l.e. $\widehat{K} = 377.898$ is close to its lower bound 246 but away from its upper bound 4250. The likelihood function suggests equal likelihood between $K = 246$ and $K = 4250$. Therefore it is more plausible that the true value of K lies in the region $(378, 4250)$ than in the region $(246, 378]$. Similarly, the m.l.e. for the peak time $\widehat{\alpha} = 19.71$ is also associated with an asymmetric likelihood based confidence interval between $\alpha = 15.5$ and 45.8. Together, they provide asymmetric scenarios in the predicted trajectories in Fig. 8.9. Although these predictions are very imprecise and not very useful, the asymmetric feature may also suggest that it is more plausible that the outbreak has not yet peaked and the final cumulative number could be in thousands. Only future data can tell.

8.3.3 *Data During the First 45 Days*

The Logistic Model: Likelihood Based Analyses

We re-fit the three-parameter logistic model to daily incidence data y_t, $t = 0, \ldots, 45$. The maximum likelihood estimates for the logistic function are

$$\begin{aligned} \widehat{\rho} &= 0.0917\ (0.0787,\ 0.105) \\ \widehat{\alpha} &= 41.29\ (41.21,\ 43.97) \\ \widehat{K} &= 1689.992\ (1422,\ 2088) \end{aligned} \tag{8.23}$$

where numbers in brackets are 95% confidence limits calculated using likelihood ratio statistics. When parameterized as

$$C(t) = \frac{i_0 K}{i_0 + (K - i_0)\, e^{-\rho t}}$$

the parameter $i_0 = C(0) = \frac{K}{1+e^{\rho\alpha}}$ has the epidemiologic meaning as the cumulative number of clinical cases by Day 0. Treating i_0 as a parameter, the maximum likelihood estimate is

$$\widehat{i_0} = 37.5\ (31.95, 43.2).$$

The expected daily incidence on Day 0 is $\widehat{C}(0) - \widehat{C}(-1) = 3.2$, as opposed to a single case on Day 0 as in the reported data.

Compared to the maximum likelihood estimates based on the first 20-day data, the extra information from Day 21 to Day 45 has resulted in remarkably improved precision for all the parameters.

The revised likelihood analysis suggests that Scenario 1 from analyses using the first 20 data points has turned out to be the most likely scenario. It is implausible that the outbreak could have peaked before Day 41. There is also evidence, at significance level 0.05, that the outbreak has peaked by Day 44. Updated data suggest a much narrower range for the uncertainty of K.

The logistic model suggests that the outbreak started approximately 30 days prior to Day 0. Since the logistic model gives a symmetric daily incidence curve, it further suggests that the outbreak will probably end around Day 115.

We update Fig. 8.9 as Fig. 8.10. The three scenarios are: (1) early peak at $\alpha_L = 41.21$, with $\rho = 0.0898$, $K = 1799$; (2) at the maximum likelihood estimates: $\widehat{\rho} = 0.0917$, $\widehat{\alpha} = 41.29$ and $\widehat{K} = 1689.992$; (3) late peak at $\alpha_U = 43.97$, with most plausible values $\rho = 0.08626$, $K = 1799$.

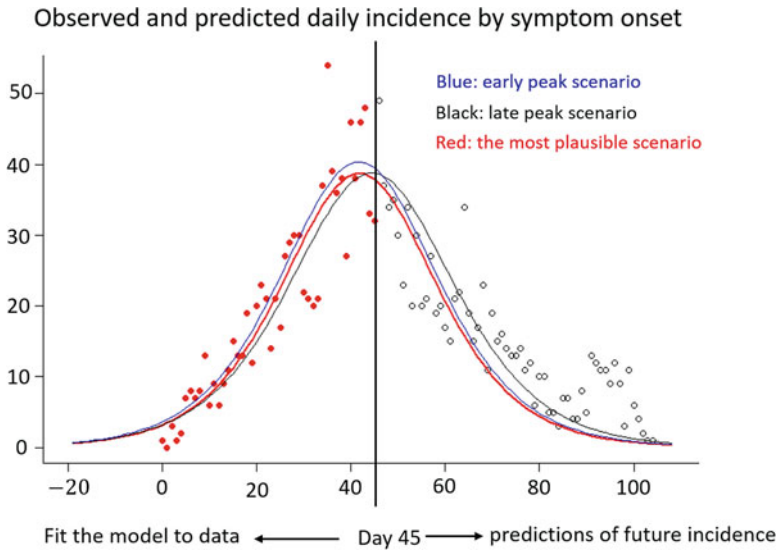

Fig. 8.10 Predictions with information from the first 45 days of data

The Logistic Model: Least Square Analysis

Least square estimates are performed based on the logistic function parameterized as $C(t) = \frac{i_0 K}{i_0 + (K - i_0)e^{-\rho t}}$. The estimated parameter values are

$$\widetilde{\rho} = 0.08922,\ \widetilde{i}_0 = 43.137,\ \widetilde{K} = 1804.4.$$

The least square method suggests that the cumulative number of infections by Day 0 was $\widetilde{C}(0) = \widetilde{i}_0 = 43.137$ and the daily incidence on Day 0 was 3.5. The estimated peak incidence time is $\widetilde{\alpha} = \frac{1}{\widetilde{\rho}} \log \frac{\widetilde{K} - \widetilde{i}_0}{\widetilde{i}_0} = 41.576$. All these estimates are in close agreement with the maximum likelihood estimates.

We compare predicted daily incidence by symptom onset based on the maximum likelihood estimation and the least square estimation from the logistic model against the observed daily incidence data as circles in Fig. 8.11. Each curve in Fig. 8.11 represents the expected values $f(t; \widehat{\Theta})$, $t = 0, \ldots, 45$. These values, together with data $(y_t, t = 0, \ldots, 45)$, are used to compute the summary measures MSE, WMSE, and Anscombe in (7.12), (7.13) and (7.14), respectively.

Residual analyses in Table 8.1 show that the least square estimates give the smaller mean square errors (MSE) by default and also slightly outperform the maximum likelihood estimates based on the sum of the squares of the Pearson residuals (WMSE). The maximum likelihood estimates perform slightly better based on the sum of the squares of the Anscombe residuals.

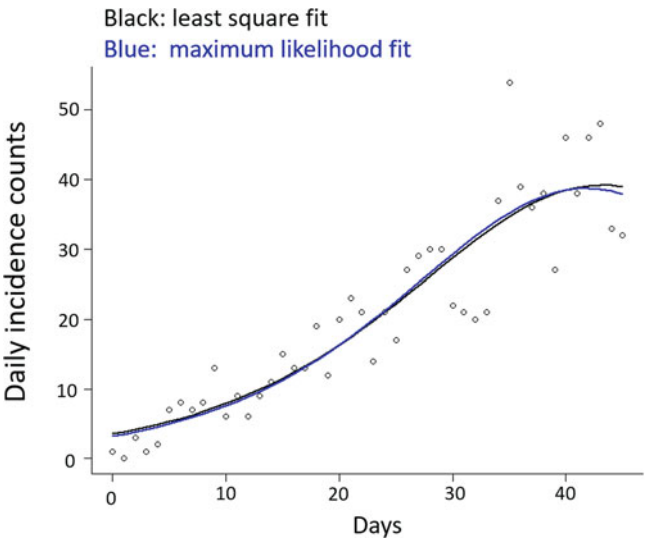

Fig. 8.11 Observed daily incidence for the first 45 days (circles) and two expected daily incidence curves as predicted by the logistic model, using the least square method (black) and the maximum likelihood method (blue)

Table 8.1 Summary residual measures (7.12)–(7.14) comparing the maximum likelihood and the least square estimates

	Maximum likelihood	Least square
MSE	32.37	32.17
WMSE	63.84	63.44
Anscombe	69.6	70.15

It is more informative to plot the residuals

$$r_t = y_t - f(t;\widehat{\Theta}),$$

$$r_t^{(P)} = \frac{y_t - f(t;\widehat{\Theta})}{\sqrt{f(t;\widehat{\Theta})}}, \qquad t = 0,\ldots,45$$

$$r_t^{(A)} = \frac{\frac{3}{2}\left[y_t^{2/3} - f(t;\widehat{\Theta})^{2/3}\right]}{f(t;\widehat{\Theta})^{1/6}}.$$

rather than their sum-of-squares. These residuals are plotted in Fig. 8.12. The plotted Anscombe residuals $r_t^{(A)}$ are approximately Gaussian distributed. Therefore the standard error lines ± 1.96 are also plotted in Fig. 8.12. The Anscombe residual plots in Fig. 8.12 detect two significant outliers for the maximum likelihood estimates.

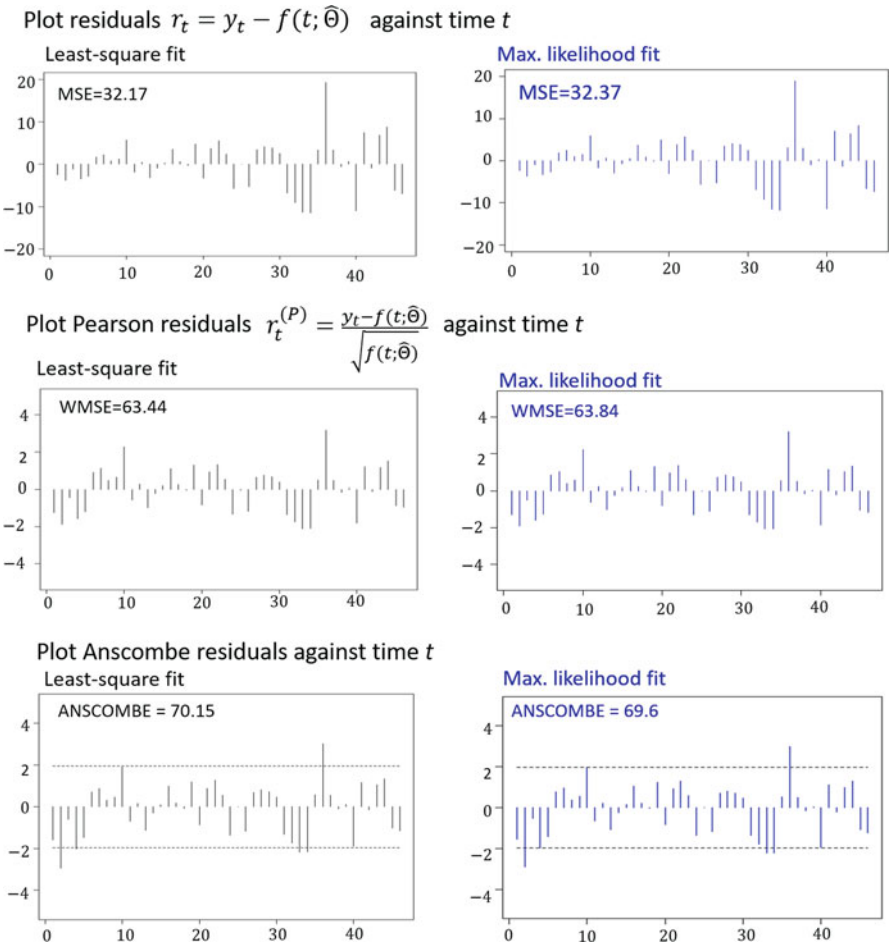

Fig. 8.12 Compare residuals between the least square estimates and the maximum likelihood estimates based on the first 45 epidemic days

Fitting Generalized Logistic Models to the First 45-Day Data with Discussions on Over-parameterization

One of the reasons to fit a generalized logistic model is to test the goodness-of-fit of the logistic model. For example, the Richards model

$$C(t) = \frac{K}{\left(1 + \left[\left(\frac{K}{i_0}\right)^{\theta} - 1\right] e^{-\rho t}\right)^{1/\theta}} \tag{8.24}$$

is the generalization of the logistic model $C(t) = \frac{i_0 K}{i_0+(K-i_0)e^{-rt}}$ when $\theta = 1$. In differential equation forms, the Richard model (as parameterized above) is the solution of

$$\frac{d}{dt}C(t) = \frac{\rho}{\theta}C(t)\left(1 - \left[\frac{C(t)}{K}\right]^{\theta}\right),\ \theta > 0 \tag{8.25}$$

whereas the logistic model is the solution of $\frac{d}{dt}C(t) = rC(t)\left(1 - \frac{C(t)}{K}\right)$, where $r = \rho/\theta$.

To test against the null hypothesis $H_0 : \theta = 1$, we conduct the likelihood ratio test based on (7.11). The value of the test statistics is

$$D = -2\left[l(\widehat{\rho}, \widehat{i_0}, \widehat{K}\ |H_0) - l(\widehat{\rho}, \widehat{i_0}, \widehat{K}, \widehat{\theta})\right] = 1.532 \tag{8.26}$$

where $l(\widehat{\rho}, \widehat{i_0}, \widehat{K}\ |H_0)$ is the value of the log-likelihood at $\widehat{\rho} = 0.0917$, $\widehat{i_0} = 37.5$ and $\widehat{K} = 1689.992$ assuming $\theta = 1$; and $l(\widehat{\rho}, \widehat{\theta}, \widehat{i_0}, \widehat{K})$ is the value of the log-likelihood of the Richards model where the maximum likelihood estimates are

$$\begin{aligned}
\widehat{\rho} &= 0.0637\ (0.0274,\ 0.086)\\
\widehat{i_0} &= 23.9\ (8.7,\ 51.8)\\
\widehat{K} &= 1999.76\ (1502.5,\ 6300)\\
\widehat{\theta} &= 0.476\ (0.132,\ 1.05)
\end{aligned} \tag{8.27}$$

Numbers in brackets are 95% confidence limits calculated using likelihood ratio statistics. The significance level for $H_0 : \theta = 1$ based on the likelihood ratio test is

$$SL = \Pr(\chi^2_{(1)} \geq 1.532) = 0.2155. \tag{8.28}$$

Discussion Although there is no evidence to reject the logistic model, the question remains whether we should discard the four-parameter Richards model which treats the additional parameter θ as a nuisance parameter, or adopt the Richards model as it may provide more valuable knowledge of public health importance.

From the point of view in favor of treating θ as a nuisance parameter, the focus is on the enormous uncertainty for the parameter of interest, such as $1502 < K < 6300$, compared to the "more precise" estimate $1422 < K < 2088$ by assuming $\theta = 1$. The argument is that information in the limited data from the first 45-days is "wasted" in the estimation of θ, which does not have direct public health interpretations as other parameters do (e.g., growth rate, initially infected number, peak time, final size). The very large uncertainty in the estimation of K, due to the inclusion of θ as a free parameter to be estimated, is not useful for public health decision makers. With this argument, the Richards model is "over-parameterized." In fact, the Richards model can be re-written in a logistic form such that $C(t)^{\theta}$ is a logistic function

$$C(t)^{\theta} = \frac{i_0^{\theta} K^{\theta}}{i_0^{\theta} + \left(K^{\theta} - i_0^{\theta}\right) e^{-\rho t}}.$$

Limited data are not informative in separating θ from K in the combined form K^{θ}. After all, the estimated θ is also associated with large uncertainty. As there is no statistical significance to reject the logistic model based on (8.28), we should discard the four-parameter Richards model.

The opposite point of view is that the significance level based on (8.28) implies that both the logistic and the Richards model fit data equally well up to Day 45 (see Fig. 8.13). It is only about the goodness-of-fit of models with respect to early part of the data, not about the important questions relating to the entire outbreak. Hence the "overly confident" estimates based on the logistic model may fail to acknowledge large uncertainties beyond Day 45. As shown in Fig. 8.13, when $\theta < 1$, the Richards model gives an asymmetric daily incidence curve with a longer tail, which is not only more realistic in most settings, but also suggests that the logistic model might have under estimated K. In fact, comparing (8.23) and (8.27), the logistic model might have under predicted approximately 300 clinical cases by the end of the outbreak. Meanwhile, the wide confidence intervals in (8.27) should be appreciated and emphasized.

At this moment in time (assuming we were on Day 45), we take notes on both arguments and move to the next phase when more data are available.

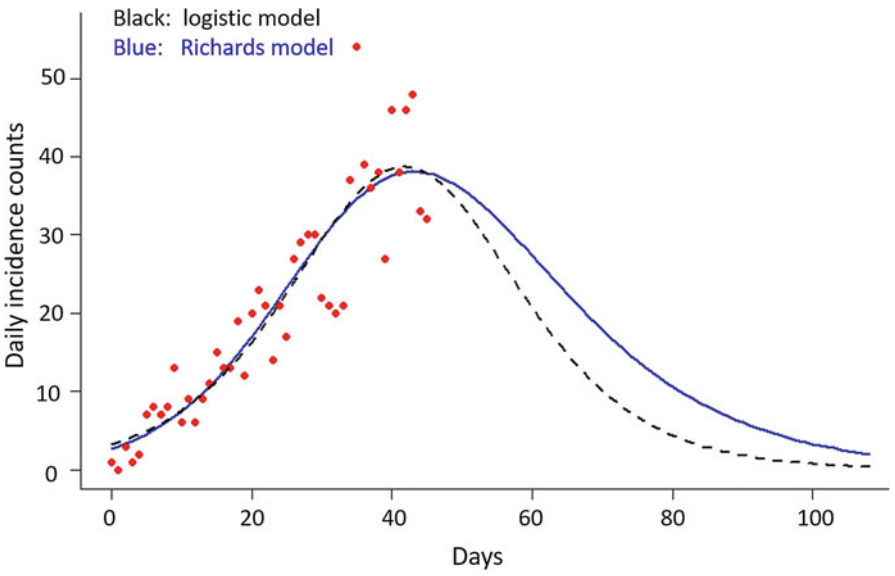

Fig. 8.13 Compare model predicted daily incidence by symptom onset based on the logistic and the Richards models, when their parameters are set at the maximum likelihood estimates. Red dots are observed data by Day 45

8.3.4 Data by Day 75

The maximum likelihood estimates for the parameters in the logistic and the Richards models are shown below:

$$\begin{array}{ll} \text{Logistic} & \text{Richards} \\ \widehat{\rho} = 0.082\ (0.0766,\ 0.0875) & \widehat{\rho} = 0.0617\ (0.0574,\ 0.0733) \\ \widehat{i_0} = 51.9\ (41.75,\ 63.75) & \widehat{i_0} = 17.36\ (7.5,\ 34.8) \\ \widehat{K} = 1805\ (1713,\ 1902) & \widehat{K} = 1852\ (1750,\ 1967) \\ H_0 : \theta = 1 & \widehat{\theta} = 0.355\ (0.152,\ 0.645) \end{array} \tag{8.29}$$

where numbers in brackets are 95% confidence limits based on the likelihood ratio statistics. The extra 30-day data, from Day 45 to Day 75, have yielded more precise estimates for all three parameters in the Richards model.

The Richards model can be also parameterized as

$$C(t) = \frac{K}{\left(1 + \theta e^{-\rho(t-\alpha)}\right)^{1/\theta}}$$

where $\alpha = \frac{1}{\rho} \log \frac{\left(\frac{K}{i_0}\right)^{\theta} - 1}{\theta}$ is the inflexion point at which $C'(t)$ is maximized. The maximum likelihood estimate for the inflexion point is

$$\widehat{\alpha} = 40.227 \text{ days } (38.36,\ 42.1).$$

The logistic model under $H_0 : \theta = 1$ gives $\widehat{\alpha} = 42.95$ days (41.8, 44.1).

Except for the estimation of K, there are significant differences in the estimation of the initial cumulative numbers $i_0 = C(0)$ and the peak time for the daily incidence α. The logistic model over predicts $i_0 = C(0)$, which also implies approximately 4 individuals developed onset on Day 0 and an earlier start of the outbreak approximately around Day-20, whereas the Richards model suggests a much smaller value for $C(0)$, approximately two individuals developed onset on Day 0 and the start of the outbreak approximately around Day-15. These are shown in Fig. 8.14, between the blue solid line and the red broken line.

By Day 75, data have shown statistical significance to reject the logistic model, corresponding to the hypothesis $H_0 : \theta = 1$. The value of the likelihood ratio statistic in (8.26) has been updated to $D = 12.902$ and $SL = \Pr(\chi^2_{(1)} \geq 12.91) = 0.0003$.

It is not appropriate to directly compare $\widehat{\rho}$ in the two models given by (8.29), because according to (8.25), the initial growth rate in the Richards model as parameterized above is the ratio $\widehat{r} = \widehat{\rho}/\widehat{\theta} = 0.1738$, in par with the m.l.e. for ρ based on the logistic model using the initial data by Day 20. This is also shown in Fig. 8.14, comparing the expected numbers of daily incidence based on the Richards model fitted to data by Day 75 with that based on the logistic model fitted to data

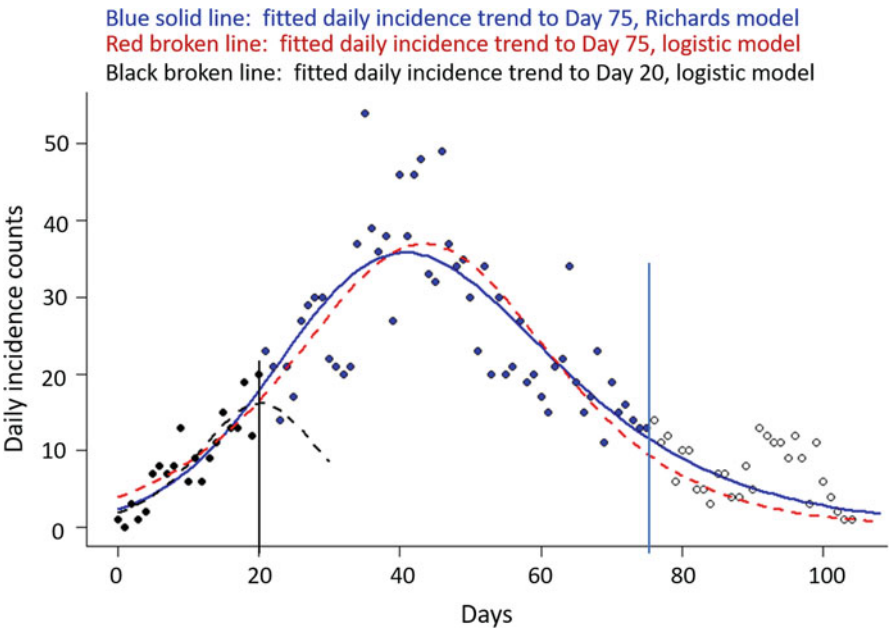

Fig. 8.14 Fitted Richards models to daily incidence counts during the first 75 days (blue dots) with comparisons with the fitted logistic model

by Day 20 (the black broken line). This is due to the asymmetry supported by the Richards model that allows for better fits on both extremes of the time-series data, whereas the logistic model is limited by its symmetric shape.

The Richards model requires a relatively large number of data points. It is not suitable as the initial model during the early phase, definitely not for data collected during the first 20 days and questionable for data collected during the first 45 days. However, as the number of data points increases, simpler models will start to misrepresent data. This will force us to adopt more complex models, not only for better prediction purposes, but also for capturing the data generating process.

We also compare the maximum likelihood estimates with the least-square estimates for the Richards model. The least square estimation yields very similar results:

$$\widetilde{\rho} = 0.0695\ (0.062,\ 0.083)$$

$$\widetilde{i_0} = 22.3\ (13,\ 31)$$

$$\widetilde{K} = 1801.9\ (1700,\ 1900)$$

$$\widetilde{\theta} = 0.52\ (0.38,\ 0.83)$$

where numbers in brackets are estimated 95% confidence limits based on 500 bootstrap samples.

Table 8.2 Summary residual measures (7.12)–(7.14) comparing the maximum likelihood and the least square estimates

	Maximum likelihood	Least square
MSE	34.08	33.6
WMSE	106.6	108.9
Anscombe	108.3	110.4

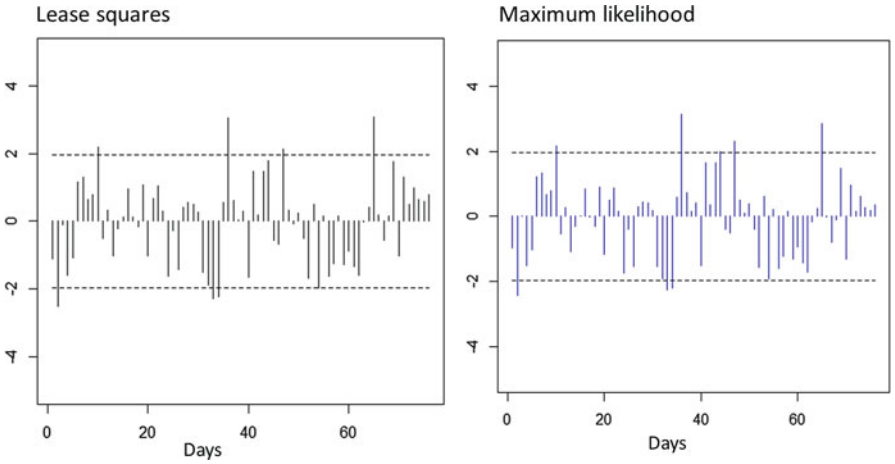

Fig. 8.15 Plots of the Ancombe residuals $r_t^{(A)} = \frac{\frac{3}{2}\left[y_t^{2/3} - f(t;\widehat{\Theta})^{2/3}\right]}{f(t;\widehat{\Theta})^{1/6}}$ for both the least square and the maximum likelihood estimates. The standard error lines ± 1.96 are based on the approximate Gaussian distribution of the Anscombe residuals

Residual analyses in Table 8.2 show that, although the least square estimates give the smaller mean square errors (MSE) by default, the maximum likelihood estimates perform slightly better based on the two other measures: the weighted mean square errors (WMSE) based on the sum of the squares of the Pearson residuals and the sum of the squares of the Anscombe residuals.

Plots of the Anscombe residuals, Fig. 8.15, reveals that both estimation methods fit data equally well. There are a few outliers in data, noticeably, on $t = 1$, 32, 33, 35, 46, 64 (days), that are either due to the inadequacy of the assumed Poisson model (i.e., over-dispersion) or the assumed Richards model. The standard errors ± 1.96 in Fig. 8.15 are based on the approximate Gaussian distribution of the Anscombe residuals.

Figure 8.16 is based on 500 bootstrap replicates of the epidemic curve based on the least square estimates, assuming the outbreak were repeated under identical conditions with Poisson error structure. The outliers on $t = 1$, 32, 33, 35, 46, 64 (days) are shown as points outside the dashed red lines indicating the 95% prediction intervals.

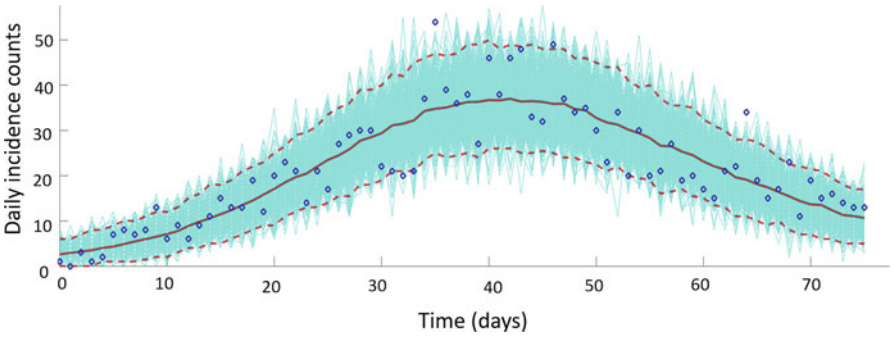

Fig. 8.16 The cyan lines correspond to 500 bootstrap replicates of the epidemic curve assuming a Poisson error structure based on the least square estimates. The solid red line corresponds to the mean, while the dashed red lines indicate the 95% prediction intervals

An additional technical note is that the least square method has been used in two different ways:

1. fitting directly to the explicit expression of the Richards model (8.24) with the four parameters (ρ, i_0, K, θ);
2. fitting the numerical solution of the differential equation (8.25) with three explicit parameters (ρ, K, θ) plus the 4th parameter $i_0 = C(0)$ as the initial condition that is also estimated.

We report back that, after careful sensitivity analyses of parameter estimates (Arriola and Hyman 2009), with respect to the initial values of the parameters in the search algorithms, and careful evaluation of the calculated values of the sum of square errors (SSE), the two fitting methods yield nearly identical numerical estimates. This comparison gives us more confidence in the least square estimates obtained directly from the numerical solution of the differential equations for other generalized logistic models in which explicit solutions do not exist.

Least Square Estimates for Other Generalized Logistic Models

We consider fitting variations of the generalized Richards model (Turner et al. 1976) with two shape parameters $\theta_1, \theta_2 > 0$:

$$\frac{d}{dt}C(t) = rC(t)^{\theta_1}\left(1 - \left[\frac{C(t)}{K}\right]^{\theta_2}\right). \tag{8.30}$$

Except for the sub-exponential model ($\theta_1 = p, \theta_2 \to \infty$), the logistic model ($\theta_1 = \theta_2 = 1$), and the Richards model ($\theta_1 = 1, \theta_2 > 0$), explicit solutions do not exist in general.

Letting $\theta_2 = 1$ and $\theta_1 = p$, we get the model defined by

$$\frac{d}{dt}C(t) = rC(t)^p\left(1 - \frac{C(t)}{K}\right), \tag{8.31}$$

which also includes a hidden parameter $i_0 = C(0)$. The least square estimation for the parameters are

$$\widetilde{r} = 0.28\ (0.21, 0.36),\ \ \widetilde{p} = 0.82\ (0.78, 0.87),$$
$$\widetilde{i_0} = 12\ (7.2, 17),\ \ \widetilde{K} = 1800\ (1700, 1900).$$

The confidence limits of the estimated parameters and the goodness-of-fit of the model are illustrated in Fig. 8.17.

Alternatively, we modify the above so that the scaling parameter p is applied to the proportion $C(t)/K$, which is more in line with the Richards model,

$$\frac{d}{dt}C(t) = rK\left[\frac{C(t)}{K}\right]^p\left(1 - \frac{C(t)}{K}\right).$$

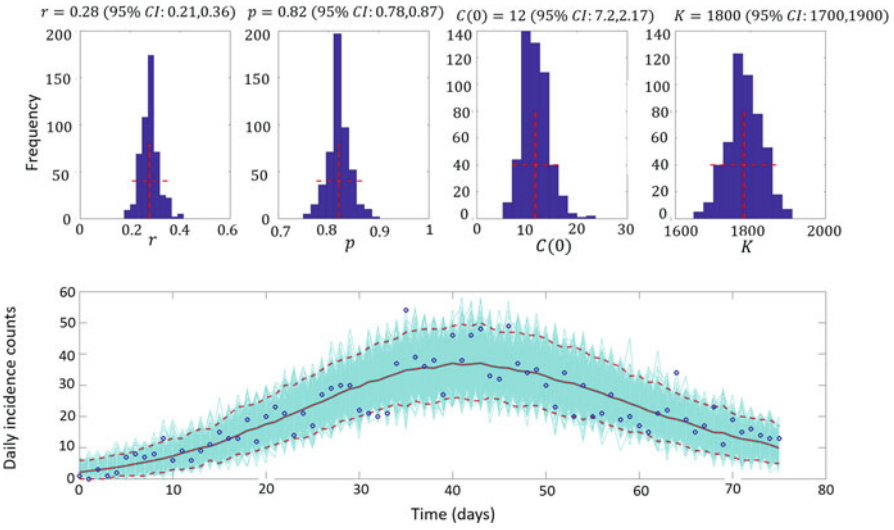

Fig. 8.17 The histograms display the empirical distributions of the parameter estimates using 500 bootstrap replicates generated assuming a Poisson error structure. The horizontal red dashed lines indicate the 95% confidence intervals of the parameter estimates. The bottom panel shows the fit of the model to the data. The blue circles are the daily incidence data. The cyan lines correspond to 500 bootstrap replicates of the epidemic curve assuming a Poisson error structure. The solid red line corresponds to mean values of the simulated sample while the red dashed lines indicate the 95% prediction intervals

Table 8.3 Summary residual measures (7.12)–(7.14) comparing three generalized logistic models with equal number of parameters

	Richards	Gen logistic 1	Gen logistic 2
	$C' = rC\left(1 - \left[\frac{C}{K}\right]^{\theta}\right)$	$C' = rC^p\left(1 - \frac{C}{K}\right)$	$C' = rK\left(\frac{C}{K}\right)^p\left(1 - \frac{C}{K}\right)$
MSE	33.6	34.5	33.9
WMSE	108.9	112.3	109.4
Anscombe	110.4	112.5	110.7

The least square estimates for the parameters are

$$\widetilde{r} = 0.073\ (0.065, 0.083),\ \ \widetilde{p} = 0.83\ (0.77, 0.9),$$
$$\widetilde{i_0} = 13\ (6.4, 21),\ \ \widetilde{K} = 1800\ (1700, 1900).$$

These two generalized logistic models have the same number of parameters as the Richards model with very similar estimated key parameters of epidemiologic interest, i_0 and K and almost equally good fit to data (Table 8.3). They do not offer more insight than the Richards model at least for this outbreak.

We also conducted the LS estimation with respect to the generalized Richards model (8.30) with parameter estimates.

$$\widetilde{r} = 0.22\ (0.18, 0.26),\ \widetilde{\theta_1} = 0.86\ (0.83, 0.89),\ \widetilde{\theta_2} = 0.95\ (0.73, 1.12),$$
$$\widetilde{i_0} = 18\ (12, 27),\ \widetilde{K} = 1800\ (1700, 1900),$$

where numbers in brackets are estimated 95% confidence limits based on 500 bootstrap samples. These estimates are very close to those based on the model (8.31) because $\widetilde{\theta_2} = 0.95\ (0.73, 0.12)$. Therefore, based on data by Day 75, it is not advisable to recommend more complex models with five parameters.

We stop this analysis at this point. In hindsight, the outbreak stopped on Day 104. The cumulative number was $K = 1852$, consistent with the m.l.e. using the Richards model fitted to data of the first 75 days. However, the Richards model could not forecast a small cluster or "a second wave" as shown in Fig. 8.14. The recorded first case remains as a single case on Day 0, which could not be captured by the models considered here.

8.3.5 Lessons Learned

1. When a new infectious disease emerges, exploratory analyses and simple phenomenological models are useful for forecasting epidemic trajectories.
2. When the number of observations is less, the initial model should be simple enough with as few parameters as possible. Over- parameterization results in undesirable large uncertainties in key parameters of interest. Among highly correlated parameters, it also leads to identifiability problems among parameters.

That is, two or more sets of parameter values yield the same expected values for data. For example, in Fig. 8.8 when $v = 0.034$, the first 20-day data equally admit the pairs of parameters: $i_0 = 40$ and $\rho = 0.1$; as well as $i_0 = 10$ and $\rho = 0.2$, corresponding to two distinct scenarios: high initial numbers with slow growth rate versus low initial numbers with fast growth rate.

3. Increasing the number of observations will, to some extent, improve the precision and identifiability among parameters in the simple model. However, beyond a certain limit, this gain will be diminished and off-set by biased estimates and lack-of-fit to data. This will force us to shift to a more complex model and closer to the data generating process. We have demonstrated this adaptive approach in the discussions while fitting models to data accumulated by Days 20, 45, and 75.
4. Even though the parameters in the simple growth curve models do not have any physical meaning (unlike those in transmission dynamic models), these simple models still need to be carefully selected and parameterized, so they can be useful in addressing key public health questions.
5. The curve models that we have employed here are highly nonlinear. The optimization algorithms to maximize the log-likelihood or to minimize the sum of square errors (SSE) are highly sensitive to the initial parameter estimates, which may lead to a local maximum or minimum. It is important to carefully evaluate the values of the log-likelihood or SSE upon convergence over a wide range of possible initial estimates.
6. Transformation of parameters does not affect assumptions of a model, but it may make interpretations more or less easy. Different ways of parametrizing the same growth function should be explored. One of the reasons is to have the parameters interpretable and aligned with public health questions. Another reason may be associated with the parameter searching algorithms. For example, parameter transformations to make the log-likelihood contours more like symmetric ellipsoids will generally facilitate numerical optimization.
7. Correlation among parameters: The "banana shaped" log-likelihood contours are typical signatures of correlation among parameters. The cross-sectional bivariate log-likelihood contour plots (e.g., Figs. 8.5 and 8.8) yield important information about correlations between pairs of important parameters.
8. When possible, graphical presentation of the likelihood surface is worthwhile, either as a 3-D function or cross-sectional log-likelihood contours. These will provide more reliable precision intervals than marginal confidence intervals for each parameter, reveal correlation among parameters, and provide better ways to communicate uncertainty. However, these are very time-consuming.
9. Approximate confidence intervals based on the likelihood ratio statistics are in agreement with the contours of the likelihood surface, as opposed to those based on standard errors which rely on a quadratic approximation. A very common feature is that these confidence intervals are highly asymmetric around their point estimates. When extremely asymmetric, the emphasis should be on the plausibility range towards the wider side of the interval rather than the point estimate. This is very important in communicating uncertainty. We demonstrated this while analyzing the Zika data during the first 20 days, with a very wide

plausibility region in favor of the slow growth pattern. This was confirmed when more data were collected by Day 45.

8.4 The Effective Reproduction Number, R_t, with Quantified Uncertainty

The basic reproduction number, commonly denoted by R_0, quantifies transmission potential in a fully susceptible population during the early epidemic take off (Anderson and May 1982). According to the classical theory of epidemics, largely based on compartmental modeling (e.g., Anderson and May 1991; Diekmann and Heesterbeek 2000; van den Driessche 2017; van den Driessche and Watmough 2002; Diekmann et al. 2010), R_0 is expected to remain invariant during the early phase of an epidemic that grows exponentially and as long as susceptible depletion remains negligible (Diekmann and Heesterbeek 2000).

In Chap. 4, Eq. (4.47): $L[g](r) = \int_0^\infty e^{-rx} g(x)dx = R_0^{-1}$ can be re-written in the renewal form

$$i(t) = R_0 \int_0^\infty g(x) i(t-x) dx \tag{8.32}$$

where $i(t) \approx e^{rt}$ is the instantaneous density of infected individuals at the very beginning of the outbreak approximated by exponential growth, and $g(x)$ is the probability density function of the (intrinsic) generation time T_G associated with the Lotka equations in Sect. 4.3.3, formally defined and further discussed as (7.18) in Chap. 7. This approximation is suitable when t is extremely small, near the disease-free equilibrium. Wallinga and Lipsitch (2007) suggested ways of estimating the basic reproduction number based on the initial growth rate r through fitting the exponential growth to early outbreak data, provided that the generation time distribution $g(x)$ is fully specified so that

$$\widehat{R}_0 = L[g](\widehat{r})^{-1}$$

where $\widehat{r}$ is the fitted initial growth rate to data.

In contrast, the effective reproduction number R_t captures changes in transmission potential over time when the system starts to move away from the equilibrium condition (Chowell et al. 2016; Nishiura and Chowell 2009). The effective reproduction number R_t is given by

$$R_t = \frac{S(t)}{S(0)} R_0$$

where $S(t)$ is the expected number of susceptible individuals in the population at time t. It is understood as the expected number of secondary infections transmitted by a typical infectious individual at calendar time t.

Nishiura and Chowell (2009) generalized the above renewal type equation through analysis of an infection-age structure model, The term "infection-age" refers to the time elapsed since infection. Define $A(t, x)$ as the rate at which an infectious individual at calendar time t and infection age τ produces secondary infections so that

$$i(t) = \int_0^\infty A(t, x) i(t - x) dx,$$

under the assumption that the relative infectiousness to infection-age is independent of calendar time (Fraser 2007), Nishiura and Chowell (2009) argue that $A(t, x)$ can be decomposed as $A(t, x) = R_t g(x)$, where $g(x)$ is the same generating time distribution as in (8.32). This leads to

$$i(t) = R_t \int_0^\infty g(x) i(t - x) dx.$$

To fit to data observed in discrete (grouped) time units over a finite period $t = 0, \ldots, T$, the following approximation

$$i(t) = R_t \sum_{x=0}^{T} g(x) i(t - x), \ t = 0, \ldots,$$

has been considered (The World Health Organization Emergency Response Team 2014, Supplementary Appendix 1; Chowell et al. 2016), where $i(t)$ is the expected number for the incidence data during the time unit t, such as daily incidence Y_t so that $E[Y_t] = i(t)$.

Assuming that the incidence up to time $t - 1$ is Poisson distributed, the daily incidence Y_t is

$$Y_t \sim Poisson \left(R_t \sum_{x=0}^{T} g(x) i(t - x) \right),$$

Then, given the incidence data as a longitudinal series denoted by $\underline{y} = (y_1, y_2, \ldots, y_T)$, the maximum likelihood estimate for R_t is

$$\widehat{R}_t = \frac{i(t; \widehat{\Theta})}{\sum_{x=0}^{T} g(x) i(t - x; \widehat{\Theta})}, \ t = 0, \ldots, T, \tag{8.33}$$

where $i(t; \Theta)$ is a suitable phenomenological model to describe the data generating process $\underline{y} = (y_1, y_2, \ldots, y_T)$, and $i(t; \widehat{\Theta})$ is the fitted incidence, provided that the generation time distribution $g(x)$ is fully specified.

Although uncertainties in parameter estimates $\widehat{\Theta}$ can be derived using the likelihood ratio statistics, establishing variance estimation for $\widehat{R}_t$ is more complex. Therefore, computer based re-sampling methods, such as bootstrapping, are preferred.

Next, we assume the sub-exponential model $i'(t) = r\,[i(t)]^p$ starting with a single individual, with the explicit form

$$i(t) = (1 + r(1-p)t)^{\frac{1}{1-p}}.$$

This model can reproduce a range of growth dynamics from constant incidence ($p = 0$) to exponential growth ($p = 1$) (Viboud et al. 2016).

We denote $(\widehat{r}^{(i)}, \widehat{p}^{(i)})$ as the estimated parameters based on the ith bootstrap sample in a re-sampling regime. Then (8.33) gives

$$\widehat{R}_t^{(i)} = \frac{i(t; \widehat{r}^{(i)}, \widehat{p}^{(i)})}{\sum_{x=0}^{T} g(x) i(t-x; \widehat{r}^{(i)}, \widehat{p}^{(i)})}, \; t = 0, \ldots, T.$$

Based on the maximum likelihood estimate (8.33) from the incidence data, a large number of bootstrap realizations create a virtual experiment with repetitions of the outbreak under identical conditions, which produce the average of $\widehat{R}_t^{(i)}$ as well as the plausible ranges for uncertainty.

8.4.1 *Example Based on the 2016 Epidemic of Yellow Fever in Two Areas of Angola: Luanda and Huambo*

For illustration, we estimated the effective reproduction number during the early phase of a yellow fever epidemic. The epidemic spread between December 2015 and August 2016 in Angola, mostly affecting the provinces of Luanda (the capital) and Huambo. Numbers of confirmed and probable reported cases are grouped into discrete time intervals on a weekly basis and assembled by the World Health Organization (The World Health Organization 2016). The corresponding time series data are available online as EXTRA MATERIALS.

For the goal of estimating R_t, we assumed a gamma distribution for the generation interval of yellow fever with a mean of 15 days (2.143 weeks) and variance of 36 days (5.143 weeks). We fitted the generalized growth model (4.61) to the growth phase of the epidemics.

The yellow fever epidemic in Luanda followed an initial growth phase consistent with exponential growth dynamics (Fig. 8.18) with the scaling of growth parameter p very close to 1.0 and our most recent estimate of the effective reproduction number at 3.3 (95%CI: 2.6, 3.6). The corresponding curves of the effective reproduction number are shown in the bottom panel of Fig. 8.18. In contrast, for Huambo, the effective reproduction number was most recently estimated at 1.2, 95% CI: 1.1, 1.4) with a relatively low scaling of growth parameter (0.36, 95% CI: 0.17, 0.55) as shown in Fig. 8.19. The curves of the effective reproduction number are shown in the bottom panel of Fig. 8.19.

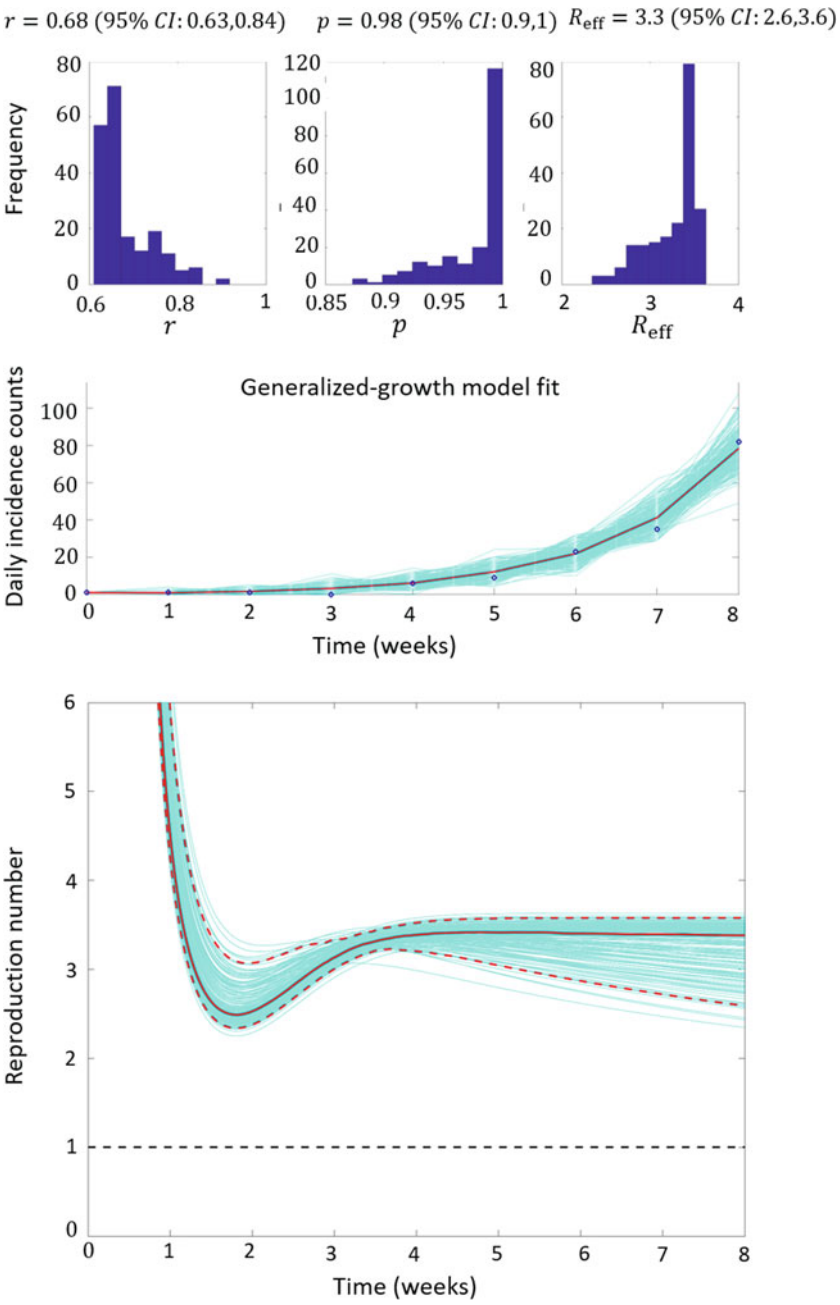

Fig. 8.18 Top panels display the empirical distributions of the growth rate, the scaling parameter, and the effective reproduction number based on fitting (4.61) to the yellow fever epidemic in Luanda, Angola. The middle panel shows the fit to the epidemic growth phase. Circles correspond to the data while the solid red line corresponds to the best fit obtained using the generalized-growth model. The blue lines correspond to the uncertainty around the model fit. The bottom panel is the weekly effective reproduction number estimated during the epidemic growth phase assuming a gamma distribution for the generation interval of yellow fever with a mean of 15 days and variance of 36

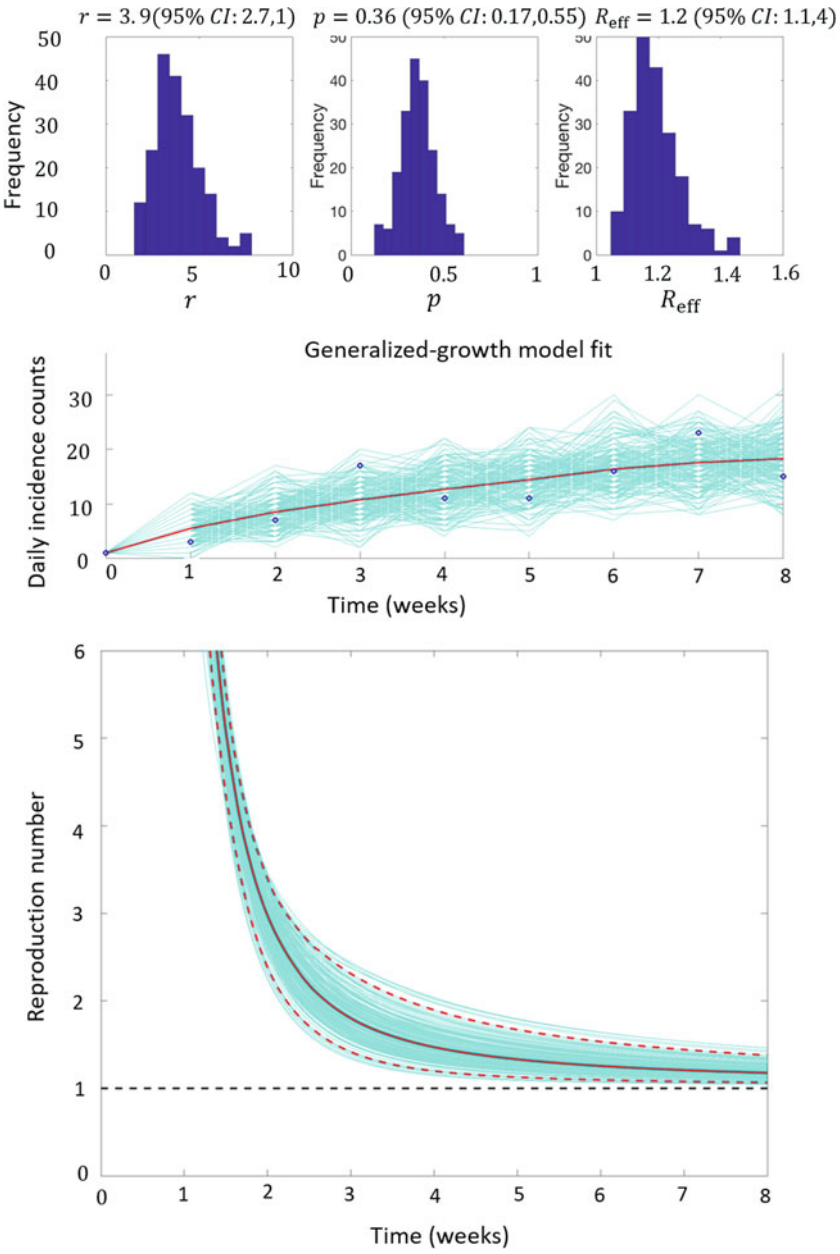

Fig. 8.19 Top panels display the empirical distributions of the growth rate, the scaling parameter, and the effective reproduction number based on fitting (4.61) to the yellow fever epidemic in Huambo, Angola. The middle panel shows the fit to the epidemic growth phase. Circles correspond to the data while the solid red line corresponds to the best fit obtained using the generalized-growth model. The blue lines correspond to the uncertainty around the model fit. The bottom panel is the weekly effective reproduction number estimated during the epidemic growth phase assuming a gamma distribution for the generation interval of yellow fever with a mean of 15 days and variance of 36

In conclusion, in this final section we have demonstrated how phenomenological models, such as the generalized-growth model, along with parameter uncertainty derived from the parametric bootstrap least-square fitting approach can be exploited to characterize transmission dynamics and their uncertainty such as the effective reproduction number through the renewal equation. Indeed, with additional data of the outbreak trajectory, we could have considered other phenomenological models such as logistic-type models and/or more elaborate error structures of the random component to account for observation correlations or data overdispersion.

8.5 Problems and Supplements

8.1 In this exercise, the reader will use phenomenological models (e.g., GGM and Richards models) to analyze the trajectory of the 2001 foot-and-mouth disease epidemic in the UK using the daily curve of the number of new infected premises. The daily number of new, real-time notifications of infected premises during the 2001 foot-and-mouth disease epidemic in the UK was obtained from the Department of Environmental and Rural Affairs (DEFRA) and is available online as an EXTRA MATERIAL. Answer the following questions:

(a) Using the GGM, what are your estimates of the growth rate (r) and the deceleration of growth parameter (p) using the first 20 epidemic days? Use maximum-likelihood estimation with a Poisson error structure.
(b) Based on your analysis in (a), assess the Anscombe residuals and compute the value of the Anscombe performance metric
(c) Based on your analysis in (a), what can you conclude from your estimate of the deceleration of growth parameter (p)?
(d) How do your parameter estimates in (a) compare with those obtained using the least-square fitting approach with a parametric bootstrap Poisson error structure?
(e) Based on your analysis in (d), assess the 95% prediction intervals around the model fit.
(f) Calibrate the Richards model to the first 10, 20, 30, or 40 epidemic days. Discuss parameter identifiability and lack of information when the model is fitted to an increasing number of observations.
(g) Using 30 and 40 epidemic days, what are the point estimates of the epidemic size? and how do these estimates compare with the actual epidemic size? What are the corresponding estimates of the epidemic peak and duration?

8.2 In this exercise, you will generate estimates of transmission potential of the 1918 influenza pandemic in San Francisco, California. The daily number of reported cases is available online as an EXTRA MATERIAL. Answer the following questions:

(a) Using the simple SEIR model without demographic factors and assuming a mean latent period of 2 days, a mean infectious period of 4 days and a population size of 550,000 provide the mean estimate and 95% confidence intervals of the basic reproduction number R_0 using 16, 18, and 20 days of the initial growth phase. For parameter estimation you can use the least square fitting approach with the Poisson parametric bootstrap which is described in Chap. 7 and illustrated with examples in Chap. 8. Note that you only need to estimate the transmission rate using your favorite technical computing language while keeping the initial number of infectious individuals $I(0)$ fixed according to the first data point. Are the R_0 estimates relatively stable during the study period?
(b) What are the corresponding values of the RMSE from your analysis in (a)?
(c) Assess the residuals and the 95% prediction intervals around the model fit and discuss your observations.
(d) Using the GGM, what are your estimates of the growth rate (r) and the deceleration of growth parameter (p) when the model is fitted to the study periods in (a)?
(e) What can you conclude from your estimate of the deceleration of growth parameter (p)? Is this parameter stable as you use 16, 18, and 20 epidemics days of data?
(f) Using your calibrated GGM based on your analysis in (d) and the approach described in Sect. 8.4, estimate the effective reproduction number R_t during the first 20 epidemic days. Compare your estimates of R_0 derived in (a) with your estimates of R_t.

8.3 Using the generalized-growth model, characterize the early ascending phase of the HIV/AIDS epidemic using monthly or annual case incidence data from any area, region, or country of the world. Answer the following questions:

(a) Using the GGM, what are your estimates of the growth rate (r) and the deceleration of growth parameter (p) when the model is fitted to the first 10 years of the epidemic?
(b) What can you conclude from your estimate of the deceleration of growth parameter (p)?
(c) Document in detail the source of your data (e.g., publication reference, website, etc.).